Ferrite Ceramics at Microwave Frequencies: Applications and Characterization

Jean-Luc Mattei, Alexis Chevalier, Vincent Laur

Ferrite Ceramics at Microwave Frequencies: Applications and Characterization

Jean-Luc MATTEI [(1)]

Alexis CHEVALIER [(1)]

Vincent LAUR [(1)]

[(1)] Lab-STICC, UMR CNRS 6285, Université de Bretagne Occidentale, Brest, France

jean-luc.mattei@univ-brest.fr

alexis.chevalier@univ-brest.fr

vincent.laur@univ-brest.fr

Keywords :

Anisotropic permeability

Demagnetizing effects

Ferrites

Gyroresonance

Microwave losses

Magnetic permeability tensor

Magnetocrystalline anisotropy

Microwave characterization

Non-reciprocal devices

Polycrystalline materials

Abstract

This article focuses on microwave ferrites and their applications. The term ferrites designates ferrimagnetic materials, which constitute a class of magnetic materials showing high dynamic permeability and high electrical resistivity over frequencies up to several GHz. This article's aim is to present a primer to polycrystalline ferrite microwave properties, including wave propagation in magnetized ferrimagnetic materials. A special emphasis is placed on the incidence of material shape on its microwave properties. Some current applications of low-loss ferrimagnets in passive microwave components are addressed. A review of some microwave characterization methods is made in the last section.

1. Ferrimagnetic materials

1.a Basic properties of polycrystalline ferrites

Ferrite materials are magnetic oxides, known as ferrimagnetic materials, which are characterized by high magnetic permeability values and insulating behavior over a wide frequency range. Their high electrical resistivity, make low-loss ferrimagnets the ideal basis for passive microwave components operating over the wide range of frequencies, from 1 to 100 GHz. They are needed in devices where non-reciprocal behavior is expected, or to strengthen the interaction between a device and the electromagnetic signal. Depending on the applications, either hard or soft ferrites are used.

Ferrites have the following main physical properties

- High electrical resistivity (of 10^5 to 10^6 MΩ.m)
- Relative dielectric constant of 11 to 17
- Low dielectric losses (of 2.10^{-4} to 15.10^{-4})
- A high magnetic susceptibility
- A Curie temperature of 200°C to 560°
- A saturation magnetization of 80 kA/m to 400 kA/m

The magnetic materials the most generally used in the microwave frequency range are polycrystalline ceramics constituted of grains (Fig.1). These are divided into magnetic domains (Weiss domains) separated by domain walls (Bloch walls). The magnetic moments are kept parallel which each other by the strong energy exchange. Their spontaneous direction of magnetization is on an easy magnetization axis. This makes it possible to minimize the magnetocrystalline energy, which is commonly described by an anisotropy field. Because of the finite size of the magnetic volume, demagnetizing effects appears. This second contribution to the total magnetic energy corresponds to demagnetizing fields, which are proportional to the magnetization. The subdivision into magnetic domains lowers the total energy of the grain.

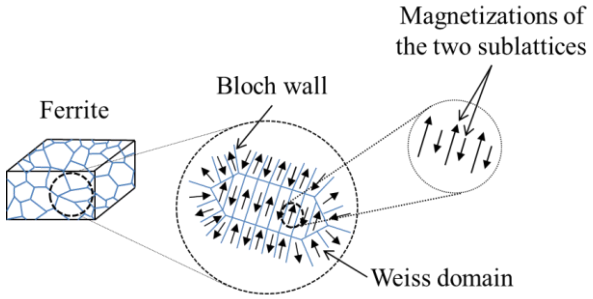

Figure 1
Polycrystalline ferrite subdivided into magnetic domains.

Ferrites are made of oxygen ions, iron ions and other cationic metals, magnetic or non magnetic. Their electrical resistivity is high, which make them worthwhile materials to be used in the microwave range. Considering their magnetic properties, in particular their magnetic saturation, magnetocristalline anisotropy and coercive field, three types of ceramics are grouped together under the heading of ferrites. There is spinel ferrites and iron garnets (that together constitute the familly of soft ferrites), and hexaferrites (that constitute the family of hard ferrites). Both spinel and iron garnets show low coercivity, low magnetocrystalline anisotropy. Whereas hard ferrites are characterized by high coercivity and high magnetocrystalline anisotropy. The ferrite crystallographic structure, for garnets as well as for spinels and hard ferrites is formed by a close-packed pattern of oxygen anions.

1.b Hysteresis loops and magnetocrystalline anisotropy

In its initial unmagnetized state, the magnetic structure of a polycrystalline material is subdivided into randomly distributed magnetic domains (the Weiss domains), separated from each other by domain walls (Bloch walls), as illustrated in Fig. 1. The variation of the magnetization M under the effect of an applied magnetic field H can be represented by a hysteresis loop that depicts the function M(H) (Fig. 2). The magnetization process is due to a combination of domain wall bowing, unpinning, displacement, and to spin rotation. More precisely, for low values of H, the volume of those domains that are the more closely oriented along the magnetic field direction expands, at the expense of the other domains, through reversible wall movement. Then, for higher values of H, expansion occurs through irreversible wall displacements. From a magnetization value close to 80% of saturation, only one magnetic domain remains. For higher values of H, spins are rotated out of their easy direction by the applied magnetic field, leading the magnetization to reach its maximum value (the saturation magnetization).

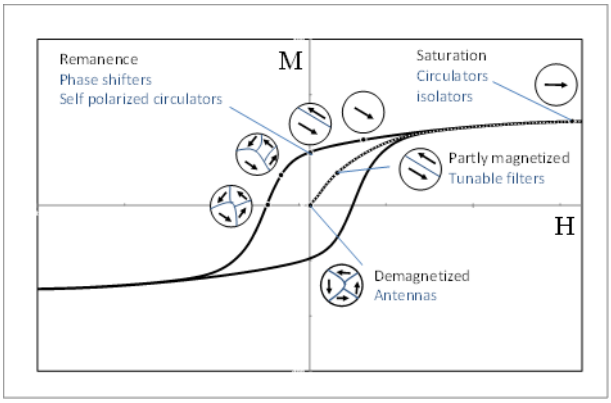

Figure 2

Hysteresis loop, and schematic representation of magnetization by domain wall movements and by spin rotation in domains. Depending on the types of applications targeted, a given magnetic material may be used in different magnetization states.

Some of the main characteristic features of a magnetic material can be deduced from its hysteresis loop: the saturation magnetization M_S, the remanent magnetization M_R, the coercive force H_C, and the anisotropy field H_A. Hard and soft magnetic materials have different typical aspects, which also depend on their texturation. (Fig. 3-4).

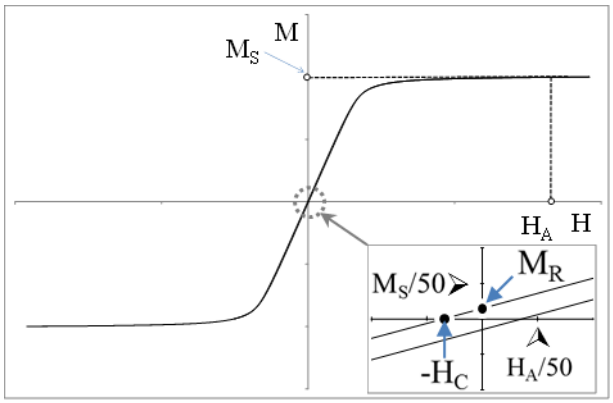

Figure 3

Typical hysteresis loop of a soft ferrite. The inset shows how the hysteresis is closed: remanence magnetization M_R and coercive field H_C are of the order of $M_S/50$ and $H_A/50$ or below, respectively. Low coercivity and low remanence reduce the energy loss associated with hysteresis.

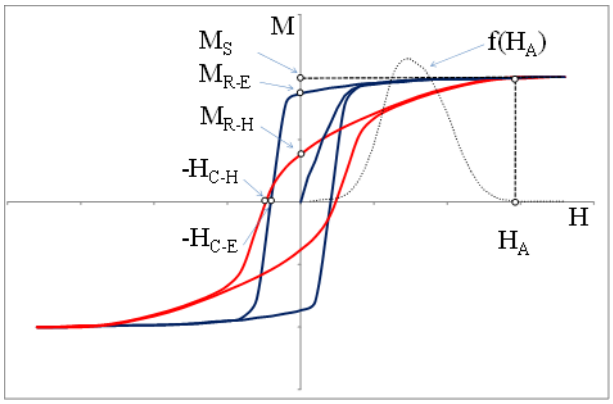

Figure 4

Typical hysteresis loops of a hard ferrite measured along the easy axis of magnetization (blue line) and in the hard plane of magnetization (red line). Their respective remanent magnetizations M_R and coercive fields H_C are labelled correspondingly: -E for easy axis and -H for hard axis measurements. The function f(A) represents the anisotropy field distribution deduced from the virgin curve, and H_A is the so-called anisotropy field (see main text for details).

Among the parameters that characterize a magnetic material, the anisotropy field, H_A, is one of the most relevant because it is a measure of the magnetic hardness of the material, that has a considerable impact on the addressed frequency range of applications. The experimental fact that magnetic properties of a material depend on the crystallographic direction along which the magnetic moments are aligned is a manifestation of the magnetocrystalline anisotropy. A first well known example is that of magnetite Fe_3O_4, which can be magnetized along the easy $\langle 111 \rangle$-like directions, while the magnetization is harder along the $\langle 100 \rangle$-like directions. A second example is that of Cobalt Co, a hard magnetic material with hexagonal structure and uniaxial magnetocrystalline anisotropy: Co can be magnetized along the $\langle 001 \rangle$-like directions, that define the easy directions of magnetization, but its hard directions of magnetization lie in the basal plane, along the $\langle 100 \rangle$-like directions (Fig. 5). In any case the anisotropy field H_A is defined as the field which saturates a particle along the direction of hard magnetization. Materials that have uniaxial symmetry are not easy to demagnetize, so they are used as permanent magnets. Because the values of H_A for hard magnetic materials are typically ten times higher than these observed for spinels, spinels are referred to as soft magnetic materials. The anisotropy field H_A is a fictive field, that allows to described the anisotropy effects from the expressions of the anisotropy energy, which is itself a function of anisotropy constants (K_1 and K_2 are the anisotropy constants of first and second order, respectively). H_A writes as follow, for the various easy directions of magnetization, as a function of K_1 :

$H_A = {}^{2K_1}/_{\mu_0 M_S}$ for the <001> easy axis, $H_A = {}^{-4(3K_1+K_2)}/_{9\mu_0 M_S}$ for the <111> easy axis and $H_A = {}^{2K_1}/_{\mu_0 M_S}$ for uniaxial materials (M_S is the saturation magnetization).

Factors that influence H_A in polycrystalline ferrites mainly consist of the misalignments of the magnetic grains, the magnetostatic interaction between them, and the existence of porosity. As a consequence, it is more appropriate to define an anisotropy field distribution $f(H_A)$ instead of than a single anisotropy field value. This distribution can be obtained from virgin curves of magnetization (Pfeiffer H. 1990). An example of $f(H_A)$ is given in Fig. 4. The highest value of the anisotropy field corresponds to the field (named H_A) at which saturation is reached, that is when the magnetizations measured along the hard and the easy directions both reach the saturation magnetization value (Fig. 5).

Depending on the types of applications targeted, a given magnetic material may be used at different magnetization states. This is illustrated in Fig. 2. With regard to the electromagnetic devices using ferrites we should mention nonreciprocal devices (circulators, isolators, etc.), the behavior of which is based on the anisotropic permeability of the magnetic material (for this point, see section 3). Tunable devices, such as filters, resonators, phase-shifters operate on the basis of the non-linear electromagnetic behavior of the ferrites when submitted to a dc magnetic field. Antennas can be miniaturized by using ferrites in a demagnetized state, where the magnetic permeability is high.

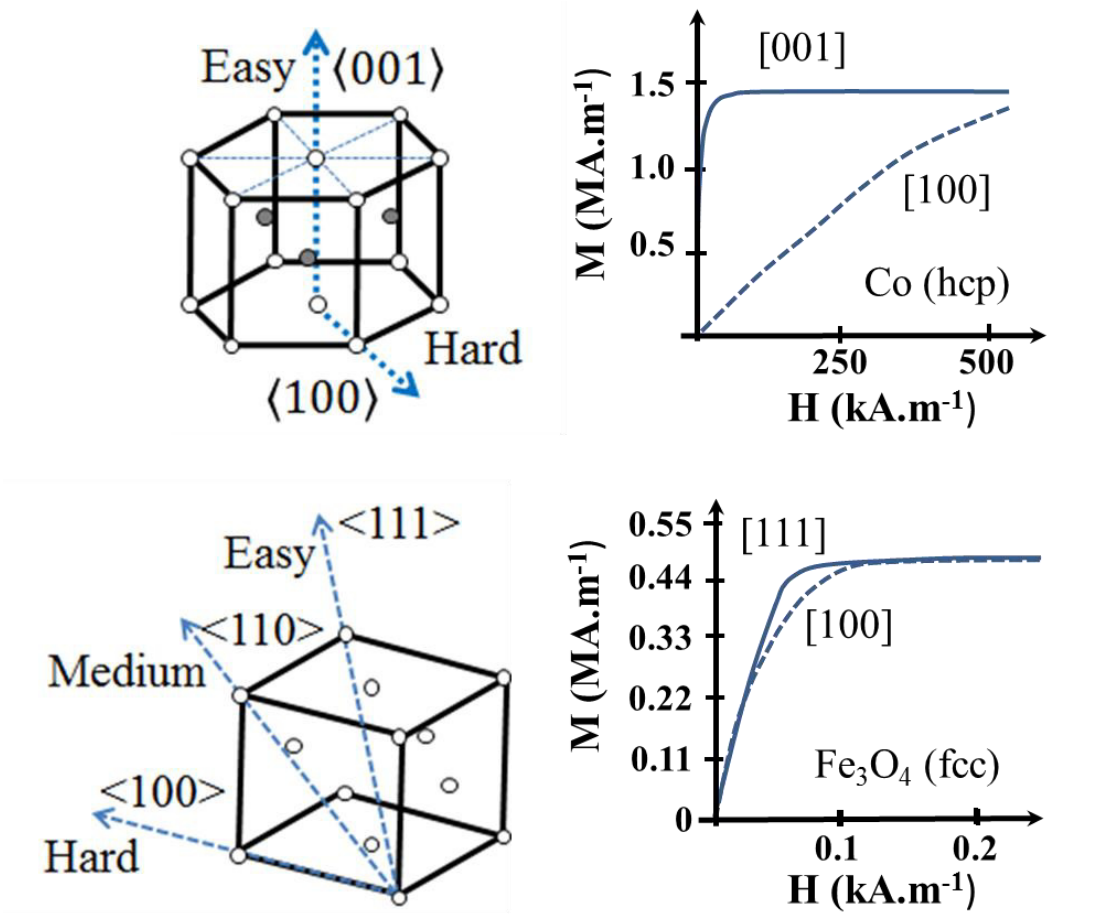

Figure 5

Up : Crystal structure and magnetization curves (300K) of a single crystal of Cobalt. <001> is the easy direction of magnetization. There are six hard directions of magnetization in the basal plane, that can be deduced by hexagonal symetry from the hard <100> direction.

Down : Crystal structure and magnetization curves (300K) of a single crystal of magnetite Fe_3O_4 (only O^{2-} ions forming a face centered cubic lattice are represented). Above 130 K, <111> is the easy direction of magnetization, <100> is the hard direction of magnetization, <110> is the intermediate direction of magnetization.

1c Soft ferrites : Garnets ferrites

Soft ferrites: Garnet ferrites

The chemical formula for garnets is $Me_3Fe_5O_{12}$, where Me represents either a trivalent metal, as Y, or a combination of metal ions such as Y-Gd or Y-Gd-Al-Co. The crystal structure is orthorombic. Among the ferrites, garnets are recommended for operating frequencies frequencies from 0.1 GHz to 100 GHz, where they show the lowest magnetic losses (ΔH<

160 $^{Am-1}$ (or 20 Oe)). This family includes Yttrium Iron Garnets (YIG), Yttrium Aluminum garnets (YAG), Calcium Vanadium Garnets (CVG), Yttrium Gadolinium Garnets (Y-Gd-G), and variants with aluminum substitutions, all of which show a remarkable degree of temperature stability over -100°C to 200°C. They are suitable for use at moderate power level. When doping with Co or Dy, YAG are usable in high power applications. Representative properties of some garnets are listed in Table 1.

Rare earths and substitutions	**Iron and substitutions**	**Doping elements**	**Saturation magnetization (M_S, kAm^{-1})**	**Curie temperature (K)**	**Resonance linewidth (ΔH, Am^{-1})**	**Off resonance linewidth (ΔH_{eff}, Am^{-1})**
Y	Fe, Al	Dy, Co	14 - 96	358 - 493	2 – 11.2	0.16 – 1.2
Y, Gd	Fe, Al	Dy, Ho	423 - 553	363 - 563	4 - 8	0.56 – 1.28
Y, Ca	Fe, Zr		156	513	0.8	1.60
Y, Ca	Fe, V, In	Dy	70	498	4.4	0.8

Table 1

Common cationic substitutions for garnets ferrites, and the associated intrinsic properties at room temperature. The presented values are taken from a number of sources, and represent what are generally taken to be the correct values for these ferrites.

1.d Soft ferrites : Spinel ferrites

The chemical fomula for spinel ferrites is $MeFe_2O_4$ where Fe is trivalent ion. Me represents either a divalent metal, either a combination of divalent metal ions, such as Mn-Mn, Ni-Zn, Ni-Al, and sometime an association of a monovalent ion (Li^+) with a trivalent ion (Fe^{3+}, Mn^{3+}). The crystal structure is clsoed packed cubic. This class of spinel ferrites splits in two subclasses, depending on the adressed frequency range. First, for frequencies lower than 1 MHz, manganese-zinc ferrites are privilegied, in reason of their high saturation magnetization (~480 kAm^{-1}), low magnetic and dielectric losses (<3.10^{-4}). However, applications above 1 MHz are not to envisaged in reason of their low electrical resistivity. The second subclass is constituted by nickel-zinc ferrites, that are suitable for use up to 500MHz due to their high electrical resistivity (10^6 MΩ.m.) The main conductivity mechanism in spinel ferrites is due to electron hopping between Fe^{3+} and Fe^{2+} ferrite (Van Uitert L. G. 1955). The effect of Fe content on the electrical resistivity of $Ni_{0.3}Zn_{0.7}Fe_{2+\delta}O_4\pm$ ferrites is shown for example in Fig. 2. Iron deficient spinel ferrites show higher resistivity than stoichiometric ones, and for this reason are highly suitable for microwave applications. In polycrystalline ferrite, grain

boundaries may also play a significant role in the electrical resistivity by limiting eddy current losses.

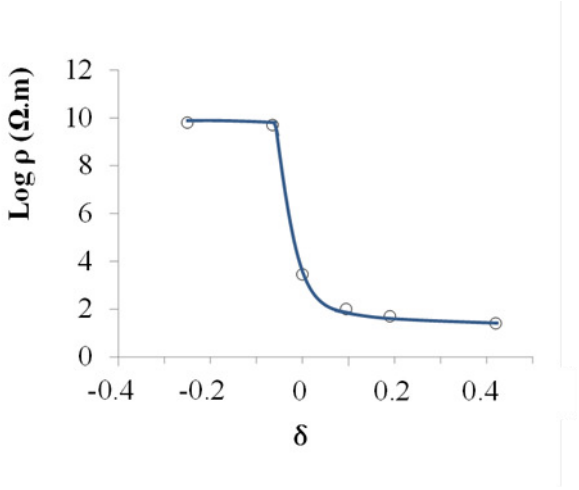

Figure 6

The dependence of resistivity (ρ) on iron stoichiometry for a $Ni_{0.3}Zn_{0.7}Fe_{2+\delta}O_4\pm$ ferrite (Adapted fromVan Uitert L. G. 1955).

Representative properties of some polycrystalline spinels are listed in Table 2 and in Table 3. The variations of the anisotropy constant K_1 and that of the anisotropy field H_A for some ferrites of formula $Ni_{1-x}Zn_xFe_2O_4$ (with K1<0) and $Ni_{1-x}Zn_xCo_{0.2}Fe_2O_4$ (with K_1>0) as a function of the Zn content are presented in figures 7a) and 7b) (from Mattei J.L. et al 2015).

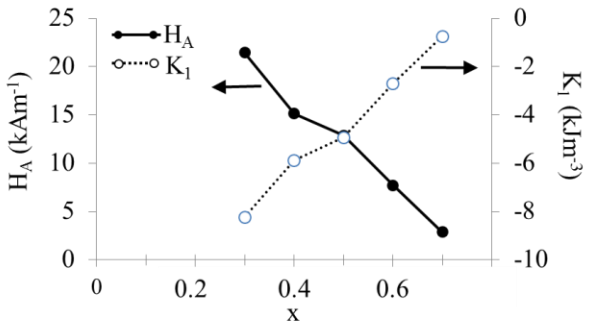

(a)

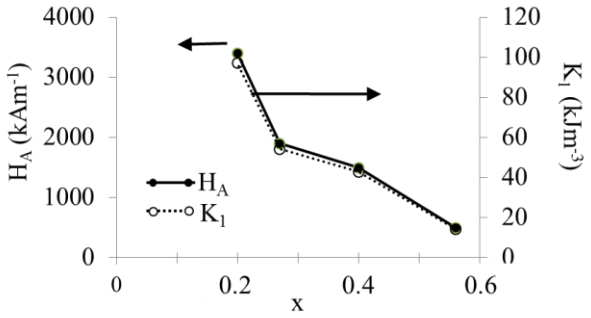

(b)

Figure 7

Anisotropy constant K_1 (dashed line) and anisotropy field H_A (full line) for some ferrites of formula (a) $Ni_{1-x}Zn_xFe_2O_4$ and (b) $Ni_{1-x}Zn_xCo_{0.2}Fe_2O_4$ as a function of the Zn content (adapted from Mattei J.L. 2015).

Molecular formula	Fe_3O_4 (a)	$NiFe_2O_4$ (a)	$Ni_{0.8}Fe_{2.2}O_4$ (a)	$CoFe_2O_4$ (a)	$MgFe_2O_4$ (a)	$MnFe_2O_4$ (b)	$Mg_{0.75}Mn_{0.25}Fe_2O_4$ (c)	$Mg_{0.25}Mn_{0.75}Fe_2O_4$ (c)
Anisotropy constant K_1 (kJm^{-3})	-11	-6.2	-3.9	200	-2.5	-3.4	-	-
Anisotropy field H_a (kAm^{-1})	24.3	24.4	20.8	500	-	180	20.8	16

Table 2

Anisotropy constant K_1 and anisotropy field H_A of some common spinel ferrites (from 1974 (a) : Valenzuela R. 1994, (b) : Srivastava C.M. and Patni M.J., (c) : Smit J. and Wijn H.P.J. 1959).

Divalent ions	Substituted trivalent ions	Saturation magnetization (M_S, kAm^{-1})	Curie temperature (K)	Resonance linewidth (ΔH, Am^{-1})	Off resonance linewidth (ΔH_{eff}, Am^{-1})
Mg, Mn	Fe	172	593	43	0.20
Mg, Mn	Fe, Al	42 - 160	363 - 563	8 - 20	0.17 - 4.20
Ni, Zn	Fe	320 - 400	448 - 473	13 - 27	1.20 - 2
Ni, Co	Fe, Al	40 - 240	393 - 858	8 - 72	1.60 – 3.20
Ni, Mg	Fe, Ti	144	773	56	> 3.60
Li, Mn	Fe	300	913	52	0.12
Li, Mn	Fe, Ti	80 - 230	573 - 773	24 - 46	0.12 – 0.72

Table 3

Common cationic substitutions for spinel ferrites, and the associated intrinsic properties at room temperature. The presented values are taken from a number of sources, and represent what are generally taken to be the correct values for these ferrites.

1.e Hard ferrites : Hexaferrites

The most commonly used hexaferrites include pure and substituted barium ferrites (BaO, $6Fe_2O_3$) and strontium ferrites (SrO, $6Fe_2O$). The crystal structure of hexaferrite is similar to that of magnetoplumbite $PbFe_{12}O_{19}$, where the Pb ion is divalent. Their anisotropy fields are two or three order of magnitude higher than that of spinels. The operational frequencies for the large range of compositionally modified hexaferrites extend from 22 GHz to 110 GHz. Because of their high coercive field and saturation magnetization ($H_c \sim 350 - 400\ kAm^{-1}$, $M_s \sim 300 - 350\ kAm^{-1}$), hexaferrites a large number of applications in magnetic recording applications and fabrication of permanent magnets. The best known are $BaFe_{12}O_{19}$ and $SrFe_{12}O_{19}$. Both are called “M-type hexaferrite”, as detailed below. They have uniaxial magnetic anisotropy, where the easy axis of magnetization is the crystallographic c-axis. Moreover, some compounds containing divalent ions, especially cobalt, have a plane of easy magnetization in the basal plane, or a cone of spontaneous magnetization at an angle between 0° and 90° with c-axis. The substitutions of Fe by Sc or In allow the anisotropy field to be lowered and the frequency range of applications accordingly extends from 4 to 40 GHz (Harris 2014).

Several other ferrimagnetic oxides are available that are derived from combinations of ferrite spinel (MeO-Fe_2O_3) M-hexaferrites (BaO-$6Fe_2O_3$) and Y-hexaferrites ($Ba_2^{2+}Me_2^{2+}Fe_{12}^{3+}O_{22}$). These are, with the nominal molecular formulae in brackets and where Me represents a divalent ion, W-hexaferrites ($Ba^{2+}Me_2^{2+}Fe_{16}^{3+}O_{27}$), Z-hexaferrites ($Ba_3^{2+}Co_2^{2+}Fe_{24}^{3+}O_{41}$), U-hexaferrites ($Ba_4\ Me_2\ Fe_{36}O_{60}$). Representative properties of some hexaferrites are presented in Table 4.

Molecular formula (abbreviation)	**Easy directions of magnetization**	**Saturation magnetization (M_S, kAm^{-1})**	**Curie temperature (K)**	**Magnetocrystalline anisotropy field (H_a, kAm^{-1})**
$BaFe_{12}O_{19}$ (BaM)	Uniaxial (c-axis)	320	723	1396
$SrFe_{12}O_{19}$ (SrM)	Uniaxial (c-axis)	345	728	1280
$Ba_2Co_2Fe_{28}O_{46}$ (Co_2X)	Cone of magnetization	272	740	760
$Ba_2Co_2Fe_{12}O_{22}$ (Co_2Y)	Planar anisotropy perpendicular to c-axis	184	613	760
$BaCo_2Fe_{16}O_{27}$ (Co_2W)	Cone of magnetization or planar anisotropy	384	703	1680
$Ba_3Co_2Fe_{24}O_{41}$ (Co_2Z)	Planar anisotropy perpendicular to c-axis	264	673	2240

Table 4

Some room temperature intrinsic properties for various hexaferrites (from Pullar R.C. 2012).

2. Magnetic permeability in the microwave range of frequencies

2.a The permeability tensor

Wave propagation in ferrites shows nonreciprocal properties arising from gyromagnetic effects, that are directly related to the precession movement of the magnetic moments. The complex phenomena involved are presented here in a simplified form.

2.a.1 Undamped precessions : From the atomic moment to the lossless ferrimagnetic material

We first consider an isolated atomic magnetic moment $\vec{\mu}$. When submitted to a dc magnetic field $\vec{H}$, the top of the magnetic moment comes to a precession movement around $\vec{H}$, described by the equation of movement: $\frac{d\vec{\mu}}{dt} = -\mu_0\gamma\vec{\mu} \times \vec{H}$, where $\mu_0\gamma = 35.18\ 10^2\ mA^{-1}s^{-1}$, γ being the gyromagnetic ratio (The value $\mu_0\gamma = 28\ GHz/T$ is also commonly used). This equation describes the precession of the magnetic moment. The source of $\vec{H}$ can be either an external bias field, an internal field (which can be a magnetocrystalline field or a demagnetizing field), or a combination of them. In the absence of an external magnetic field, a precession can be brought about by the internal magnetic field produced by the total magnetic anisotropy.

Turning to the case of a ferromagnetic material constituted of an assembly of magnetic moments, the dc magnetic field is supposedly large enough to bring magnetization to saturation ($\overrightarrow{M_S}$). Because the molecular field, which represents the interaction exchange is parallel to each magnetic moment, the previous equation is validly extended to: $\frac{d\overrightarrow{M_S}}{dt} = -\mu_0\gamma\overrightarrow{M_S} \times \vec{H}$, which describes the precession of the saturation magnetization. In addition, if an AC magnetic field $\vec{h}$ is applied in the plane perpendicular to $\vec{H}$, the equation of motion of $\overrightarrow{M_S}$ can be written

$$\frac{d\vec{M}}{dt} = -\mu_0\gamma\vec{M} \times (\vec{H} + \vec{h}) \tag{1}$$

where the magnetization $\vec{M}$ is the sum of $\overrightarrow{M_S}$ with a variable component $\vec{m}$: $\vec{M_s} = \vec{M} + \vec{m}$. This equation is valid for an infinite medium, where no demagnetization due to the shape of the magnetic volume needs to be taken into account, and assuming that the precession is not damped. The variable component $\vec{m}$ supposedly has the same harmonic time dependance than the field $\vec{h}$ (i.e., $e^{j\omega t}$). The relationship between $\vec{m}$ and $\vec{h}$ can be written $\vec{m} = \bar{\bar{\chi}}\,\vec{h}$, where $\bar{\bar{\chi}}$ is the tensorial relative susceptibility. Solving equation (1), within the hypothesis framework of $|\vec{h}| \ll \left|\overrightarrow{H_{DC}}\right|$ and $|\vec{m}| \ll |\vec{M}|$, leads to the classical formulation of the susceptibility tensor $\bar{\bar{\chi}}$, according to Polder (Polder D.), or alternatively to the Poder's relative permeability tensor $\bar{\bar{\mu}} = 1 + \bar{\bar{\chi}}$. Its conventional expression for a magnetic field bias $\vec{H}$ arbitrarily directed along the z-direction is

$$\bar{\bar{\mu}} = \begin{bmatrix} 1+\chi & j\kappa & 0 \\ -j\kappa & 1+\chi & 0 \\ 0 & 0 & 1 \end{bmatrix} \tag{2}$$

where

$$\chi = \frac{\omega_0\omega_m}{(\omega_0^2 - \omega_m^2)} \tag{3a}$$

$$\kappa = \frac{\omega_m\omega}{(\omega_0^2 - \omega_m^2)} \tag{3b}$$

and with $\omega_0 = \gamma|\vec{H}|$ and $\omega_m = \gamma|\vec{M}_s|$.

$\bar{\bar{\chi}}$ relies on the AC magnetic field $\vec{h}$, conveyed by the electromagnetic wave, to the dynamic magnetic moment $\vec{m}$ that was generated in the material. The set of equations (2) and (3) means that the energy absorption by the material from an electromagnetic wave of pulsation ω is maximal when the static field is equal to ω_0. The gyromagnetic pulsation ω_0 is also known as the Larmor pulsation, and $f_0 = \omega_0/2\pi$ is the natural ferromagnetic resonance (NFMR) of the ferrite. This model describes the AC susceptibility (or permeability) of a ferromagnetic material of infinite size and magnetized at saturation. However, in real situations magnetic losses are involved. This aspect will be discussed in the next section.

In the case of a ferrimagnetic material, two magnetic sublattices are present, each of which is characterized by different magnetizations and molecular fields. This situation presents a similar problem to that of two coupled oscillators. Consequently, there are two resonance frequencies, the first lying in the far infrared, which is beyond the scope of this article. The general expression of the second magnetic resonance frequency of the two-sublattice model has the same form as that originally obtained for the ferromagnetic case (Wangsness R. K. 1954, Smit J. and Wijn H.P.J. 1959).

2.a.2 Damped precession : a dissipating behavior

In the above section our basic assumptions were firstly that the precession movement of the magnetization was undamped, secondly that the material was magnetized at saturation, and thirdly that the material has infinite dimensions. In the most general case, at least two of these assumptions are not fulfilled. Let us first consider precession damping. Interactions take place in the magnetic material, firstly inside the system of spins itself, and secondly between the system of spins and its surroundings. These interactions cause a damping of the magnetization precession movement. Several phenomenological models introduced damping into the former relation (1), in order to reflect the existence of forces resulting in a sharper angle between the magnetic moment and the DC field (Fig. 6). This is described by the Landau-Lifschitz-Gilbert (L-L-G) equation (Landau L and Lifshitz E. 1935, Gilbert T. L. 1955):

$$\frac{d\vec{M}}{dt} = -\mu_0\gamma\vec{M} \times \left(\vec{H} + \vec{h}\right) + \alpha\vec{M} \times \frac{d\vec{M}}{dt} \qquad (4)$$

Coefficient α is a phenomenological factor, that characterizes the damping behavior of the magnetic moments. The permeability tensor remains in the form expressed by relation (2). The diagonal and extra-diagonal terms (χ and κ) can now be written:

In this relation $\vec{H}$ is the total bias static magnetic field, and $\vec{h}$ is the magnetic field conveyed by the plane electromagnetic wave, with angular frequency ω. Coefficient α is a

phenomenological factor, that characterizes the damping behavior of the magnetic moments. The permeability tensor remains in the form expressed by relation (2). The diagonal and extra-diagonal terms (χ and κ) can now be written:

$$\chi=\frac{\Omega_0\omega_m}{(\Omega_0^2-\omega_m^2)} \tag{5}$$

$$\kappa=\frac{\omega_m\omega}{(\Omega_0^2-\omega_m^2)} \tag{6}$$

where the complex angular resonance frequency Ω_0 is writen:

$$\Omega_0=\omega_0+j\omega\alpha \qquad \text{with } \omega_0=\gamma H \tag{7}$$

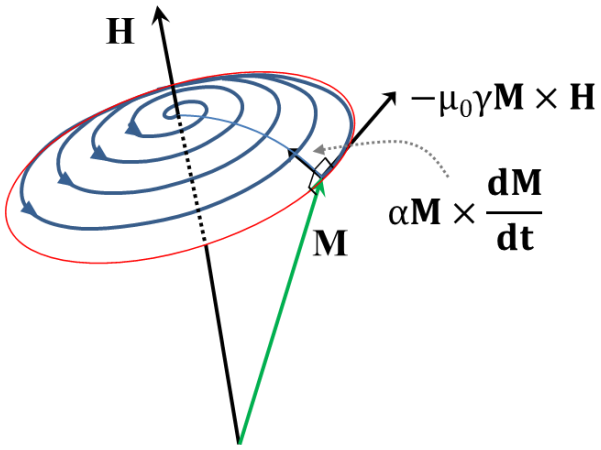

Figure 8

Precessional dynamic of magnetization, with phenomenological damping.

The effect of damping on the diagonal (μ) and extra-diagonal (κ) terms of the magnetic susceptibility tensor is shown in Fig. 9. The angular resonance frequency ω_R, that corresponds to the frequency at which μ'' and κ '' reach their maximum value, depends on the damping factor according to the relationship $\omega_R^S=\frac{\omega_0}{\sqrt{1+\alpha^2}}$.

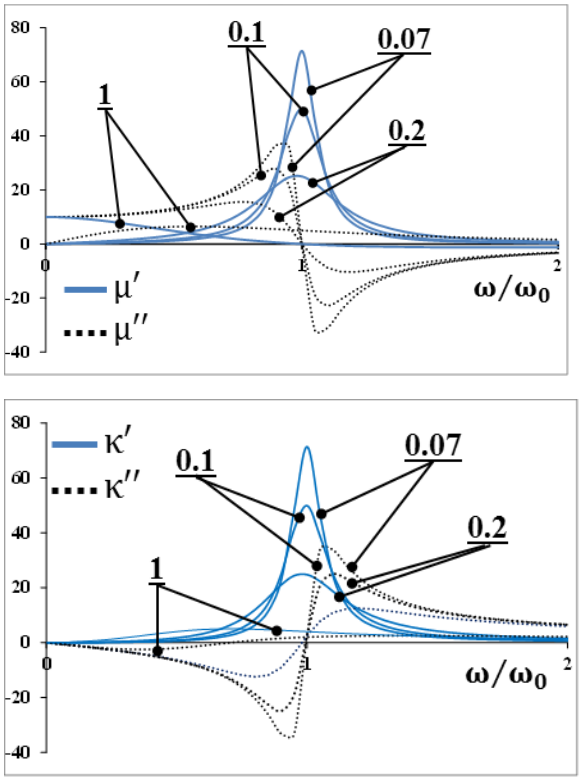

Figure 9

Incidence of the damping factor α on the magnetic permeability spectra $\mu(\omega/\omega_0)=1+\chi(\omega/\omega_0)$, where χ is given by equation 5a, ploted in reduced units of angular frequency (ω_0 is the angular resonance frequency without damping). Real part (full lines) and imaginary part (dashed lines) of μ and κ are presented for different values of α (0.07, 0.1, 0.2, 1), as indicated in the figure.

2.a.3 The frequency dispersion of permeability spectrum μ(f)

For polycrystalline ferrites, the frequency dispersion μ(f) of permeability spectrum can be assigned to and described by the superposition of two types of magnetizing processes, spin rotation and domain wall motion (Rado G. 1953) :

$$\mu(f) = \mu_S + \mu_{DW} = 1 + \chi_S + \chi_{DW}$$

The first contribution is given by the damped spin rotation. When derived from Eq. (5) and Eq. (7), real part and imaginary part of spin rotation susceptibility are described by Eq. (8-9) here below.

$$\chi_S' = \chi_S^{stat} \frac{\left[\left(1-\frac{\omega^2}{\omega_0^2}(1-\alpha^2)\right)\right]}{\left[\left(1-\frac{\omega^2}{\omega_0^2}(1+\alpha^2)\right)\right]^2 + 4\alpha^2\frac{\omega^2}{\omega_0^2}} \quad (8)$$

$$\chi_S'' = \chi_S^{stat} \frac{\omega}{\omega_0}\alpha \frac{\left[\left(1+\frac{\omega^2}{\omega_0^2}(1+\alpha^2)\right)\right]}{\left[\left(1-\frac{\omega^2}{\omega_0^2}(1+\alpha^2)\right)\right]^2 + 4\alpha^2\frac{\omega^2}{\omega_0^2}} \quad (9)$$

These expressions include three parameters : the spin damping factor α, the natural angular resonance frequency ω_0, and the DC spin rotation susceptibilityχ_S^{stat}.

The second contribution arises from magnetization process associated with domain-wall displacement. Real part and imaginary part of domain wall susceptibility are described by Eq. (10-11), that were established from an analogy with the harmonic oscillator (Perekalika T.M. et al. 1961, Mikami I.1973):

$$\chi_{DW}' = \chi_{DW}^{stat} \frac{\left(1-\frac{\omega^2}{\omega_{DW}^2}\right)}{\left(1-\frac{\omega^2}{\omega_{DW}^2}\right)^2 + \beta^2\frac{\omega^2}{\omega_{WD}^2}} \quad (10)$$

$$\chi_{DW}'' = \chi_{DW}^{stat} \frac{\beta\frac{\omega}{\omega_{DW}}}{\left(1-\frac{\omega^2}{\omega_{DW}^2}\right)^2 + \beta^2\frac{\omega^2}{\omega_{WD}^2}} \quad (11)$$

The involved parameters are the wall damping factor β, the angular relaxation frequencyω_{DW}, and the DC wall susceptibilityχ_{DW}^{stat}.

The angular frequency ω_R^{DW} where χ_{DW}'' reaches it maximum value is given by the relation :

$$\omega_R^{DW} = \omega_{DW}\sqrt{\frac{1}{3}\left[1-\frac{\beta^2}{2}+\sqrt{\left((1-\frac{\beta^2}{2}\right)^2+3}\right]}$$

The measured permeability of a $Ni_{0.5}Zn_{0.3}Co_{0.2}In_{0.02}Fe_{1.98}O_4$ polycrystalline material was fitted (Fig.10) assuming that the permeability spectrum is the superposition of these two contributions to magnetization process. The first one was attributed to spin rotation, which is grain-size independant. Opposite, the second one, attributed to domain walls motion, depends on the grain size (Goldman A. 2006). It was observed by experimental means that the grain

size distribution presented two maxima, both over the single-domain grain size value. Accordingly a satisfactory fit was obtained when, in addition to the spin rotation contribution, two domain wall contributions were involved.

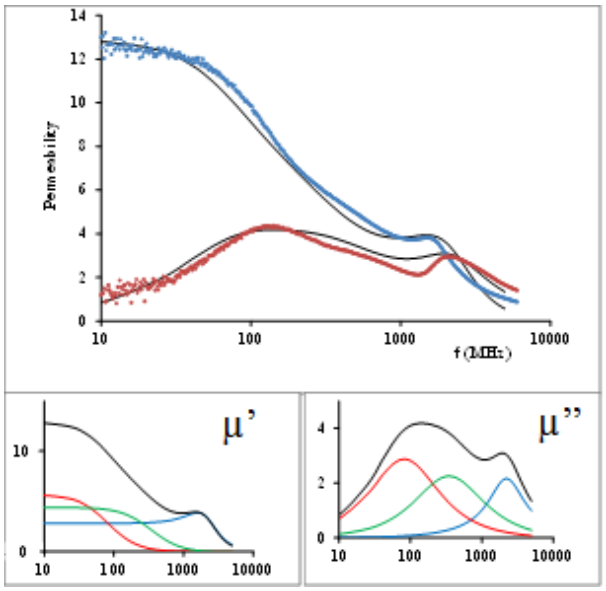

Figure 10

Permeability spectra of a $Ni_{0.5}Zn_{0.3}Co_{0.2}In_{0.02}Fe_{1.98}O_4$ sintered ferrite. Upper figure : Experimental values are denoted by symbols. Solid lines show total permeability combined with spin rotation and domain wall motion components (black lines). Their respective contributions to the total real permeability (μ') and imaginary permeability (μ'') (both in black lines) are detailed in the lower figures : spin rotation (blue lines) and domain wall motion (red and green lines).

In practice, even though the absorption peak that appears on the spectra of the imaginary parts of the permeability tensor components is well described by the Polder formulations if the magnetic body is saturated, the actual absorption peak is much broader in the case of a demagnetized state and is, moreover, shifted through higher frequency values for partially magnetized state. This is mainly due to two effects directly linked to the shape of the magnetic volume, and to its subdivision in magnetic domains, that were not yet taken into account. These points are addressed in the following section.

2.a.4 Shape demagnetizing effects

When establishing equations (3), the strong hypothesis was made that the applied DC field intensity was high enough to cause the disappearance of the magnetic domains and the magnetic moment alignment in its direction. Consequently, the internal magnetic field was considered to be constant throughout the magnetic volume. Then, neither the shape of the sample nor its aspect ratio were taken into account. From a strict point of view, Polder's

model is therefore valid only at the scale of the saturated ferrite of infinite size. However, the resonance frequency actually depends for a large part on the geometrical characteristics of the sample. In order to extend the validity of Polder's model to materials of finite size, Kittel took into account the shape demagnetizing effects, which directly depend on the shape of the material. Regarding the case of ideal ellipsoidal shaped material, the demagnetization contribution to the internal magnetic field for an isolated and uniformly magnetized volume, is the dipolar demagnetizating field $\vec{H}_d$ that is expressed as: $\vec{H}_d = -\overline{\overline{N}}\vec{M}$. $\vec{H}_d$ is in opposite direction to the applied field. The diagonal demagnetization tensor $\overline{\overline{N}}$ is defined so that its diagonal components verify $N_x + N_y + N_z = 1$. The N_is are geometric factors, known as demagnetizing factors or demagnetization coefficients. At every magnetic core of finite dimensions, the demagnetizing field reduces the external field (Except for a closed toroidal core of homogeneous full material submitted to an external field with the orthoradial symmetry, allowing the closure of the magnetic flux lines). For an ellipsoid with the static magnetic field in the z-direction, the internal field is uniform, it can be written as $\vec{H}_i = \vec{H} + \vec{H}_d$ and Kittel's equation gives the resonance pulsation (also named FMR: Ferrimagnetic Resonance Frequency):

$$\omega_0 = 2\pi\mu_0\gamma\sqrt{(H + (N_x - N_z)M_z)\big(H + \big(N_y - N_z\big)M_z\big)} \tag{12}$$

Demagnetization coefficients are well-known for some ideal shapes of ferrites (Table 5). For example, demagnetization factors of sphere are the same in the three Cartesian directions, $N_x = N_y = N_z = 1$. Regarding equation (12), FMR of a ferrite sphere will be similar to that of an infinite material, which is why sphere samples are used to extract the intrinsic properties of ferrites, such as their anisotropy field. For a flat cylinder with the z-axis perpendicular to its surface, $N_x = N_y = 0$ and $N_z = 1$. Following equation (12), FMR will be lower than the one of an infinite material.

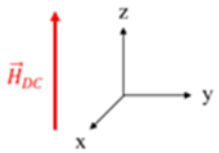

	N_x	N_y	N_z
Sphere 	1/3	1/3	1/3
Flat cylinder 	0	0	1
Long cylinder 	1/2	0	1/2
Thin slab 	0	0	1

Table 5

Demagnetization coefficients for different standard shapes of ferrites.

N_i coefficients can be rigorously calculated for ellipsoidal shapes, but only estimated for other shapes. Numerical values of demagnetizing factors have been calculated for ellipsoids (Osborn J. A 1945), for circular cylinder (Chen D.X et al 1991), and for rectangular prisms (Aharoni A. 1998).

In the case of rectangular prisms, whose dimensions are 2a, 2b and 2c (Fig. 11), Aharoni proposed analytical formulas that make it possible to estimate demagnetization coefficients along the three Cartesian coordinates. In general, these equations are complex. In the particular case of a square cross section, a = b, the Nz coefficient can be calculated using the following equations:

$$\pi N_z = \left(p - \frac{1}{p}\right) ln\left(\frac{\sqrt{p^2+2}+1}{\sqrt{p^2+2}-1}\right) + \frac{2}{p} ln\left(\sqrt{2}+1\right) + p\, ln\left(\frac{\sqrt{p^2+1}-1}{\sqrt{p^2+1}+1}\right) + 2\, arctan\left(\frac{1}{p\sqrt{p^2+2}}\right) + \frac{2(1-p^2)}{3p}\sqrt{p^2+2} + \frac{2(1-p^3)}{3p} - \frac{2^{3/2}}{3p} \quad (13)$$

where $p = {}^{c}/_{a}$.

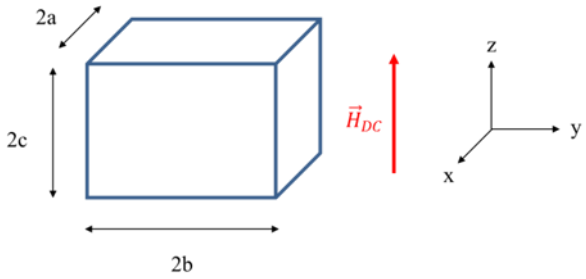

Figure 11

Rectangular prism with a DC field applied along z-axis.

The evolution of N_z coefficient of a square prism (a = b) as a function of shape factor p calculated using Aharoni equations is shown in Fig. 10. For low values of p, the case corresponding to a flat plate, N_z is close to 1 in accordance with Table 2. The special case of a cube (a = c leading to p = 1) leads to a value of 1/3, similar to the case of a sphere.

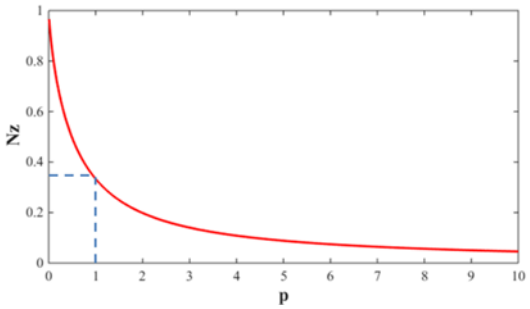

Figure 12

Evolution of the N_z coefficient as a function of p=c/a in the case of a rectangular prism with a=b (calculated from Aharoni's equations).

For a flat cylinder, a shape that is mostly used in microwave circulators, Helszajn (Helszajn J. 2008) established relationships between the thickness of a cylinder H, its radius R, and approximate demagnetizing coefficients along the three Cartesian coordinates, as follows:

$$N_z \approx 1 - \left(\frac{H}{2R}\right)\left[1 + \left(\frac{H}{2R}\right)^2\right]^{-1/2} \tag{14}$$

$$N_x \approx N_y \approx \frac{1}{2}(1 - N_z) \tag{15}$$

As an example, for a thin disk with a height H = 0.1 mm and a radius R = 1.25 mm, these formulas give: N_z = 0.959, N_x = N_y = 0.02. Such a flat cylinder gives rise to a strong demagnetizing field along the z-direction so that internal field will be lower than the applied field.

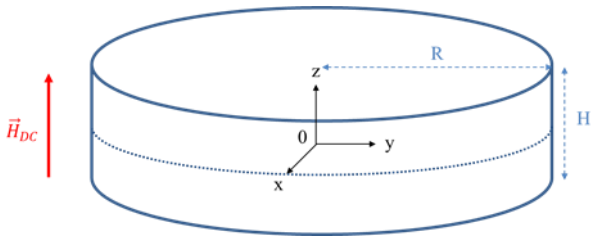

Figure13

Ferrite cylinder with a DC field applied along z-axis (radius R and thickness H).

An ellipsoid has the property that when a uniform DC magnetic field is applied to it, the demagnetizing field is uniform throughout the sample. In practice, however, the shape of the ferrite sample is rarely an ellipsoid, consequently nonuniformity of the internal field is most frequent. Ferromagnetic bodies with arbitrary shapes do not have uniform spatial distribution of demagnetizing fields and Nz coefficient calculated by using Aharoni formulas is only an approximation. An example of the spatial distribution of the internal magnetic field for a ferrite puck polarized by a uniform external magnetic field is presented in Fig. 14. If this internal field inhomogeneity is not taken into account, it may have a detrimental impact on the operations of the device that would use such a ferrite. This will be presented in greater details here below.

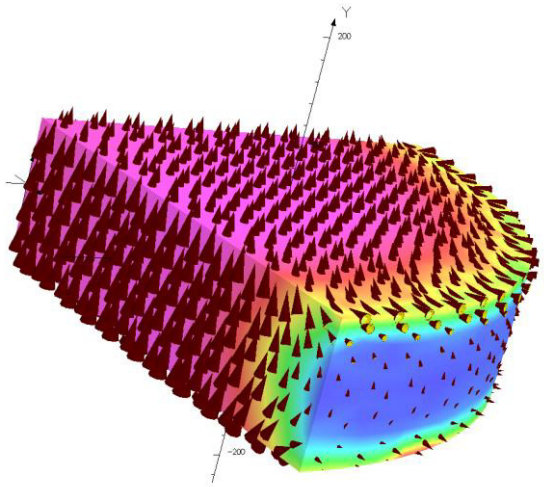

Figure 14

Example of the spatial distribution of the internal magnetic field for a ferrite puck polarized by an uniform external magnetic field (analysis performed by using OPERA3D packages, OPERA3D, Vector Fields).

Analytical equations making it possible to calculate the evolution of N_z coefficient as a function of the radius in a flat cylinder of ferrite under a uniform DC magnetic field were proposed by (J. Helszajn 2008). In this model, two different equations are used to calculate $N_{z,center}$ at the center of the sample and $N_{z,edge}$ at its edge (Joseph R.I.and Schlöemann E. 1965). Helszajn later unified this set of equations in order to calculate the spatial distribution of N_z in a disk of ferrite.

$$N_{z,center}(r,0) = 1 - \frac{(H/2R)}{\left[1+\left(1+(H/2R)^2\right)\right]^{1/2}} - \left[\frac{3(H/2R)}{\left[1+\left((H/2R)^2\right)\right]^{3/2}} - \frac{3(H/2R)^3}{\left[1+\left((H/2R)^2\right)\right]^{5/2}}\right]\left(\frac{r}{2R}\right)^2 \quad (16)$$

$$N_{z,edge}(r,0) = \frac{1}{2} + \left(\frac{1}{\pi}\right) tan^{-1}\left[\left(\frac{2R}{H}\right) - \left(\frac{2r}{H}\right)\right] \quad (17)$$

$$N_{z,global}(r,0) = \left(N_{z,center} - N_{z,edge}\right)\left[1 - (r/R)^4\right] + N_{z,edge} \quad (18)$$

Figure 15 shows the evolution of the N_z coefficient as a function of the ratio between the distance to the center r and the radius R of a ferrite disk. This calculation was performed for a flat disk of thickness H = 0.1 mm and radius R = 1.25 mm. These results demonstrate that demagnetization coefficients are strongly inhomogeneous in such ferrite disks with a strong decrease from the center of the disk (N_z = 0.96) to the edge (N_z = 0.5).

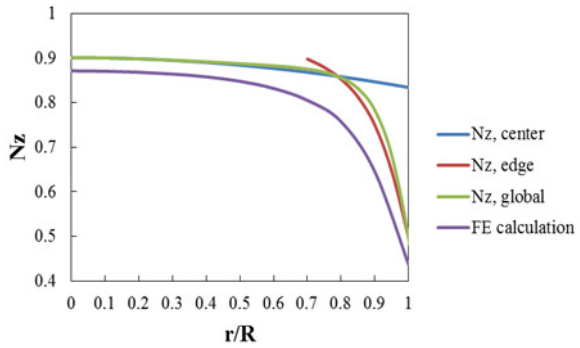

Figure 15

Demagnetizing factor of a flat cylinder as a function of the distance to the center r/R calculated using equations (8)-(10) and compared with FE simulation.

This variation was compared with Finite-Element (FE) calculation. The simulation was performed for a flat ferrite disk with the same geometry (H = 0.1 mm, R = 1.25 mm), a saturation magnetization M_s = 23873 $A.m^{-1}$ under a uniform applied static magnetic field H_{DC} = 70000 $A.m^{-1}$. The variation of N_z as a function of r/R at the mid-height of the disk is shown in Fig. 16. Although the trend is similar to the model proposed by Joseph, Schlöemann and Helzasjn, one should note that the values are slightly lower.

In reality, the situation in such ferrite samples is actually more complex than a single variation of a demagnetizing field in the plane of the disk. Figure 16 thus shows the spatial distribution of demagnetizing coefficient N_z parallel and perpendicular to the plane of a ferrite disk. Even for a disk with a very low thickness to height ratio H/R, one should note a non-negligible variation of N_z along the thickness of the disk, thus inducing a different spatial distribution of N_z at the top and the middle of the sample.

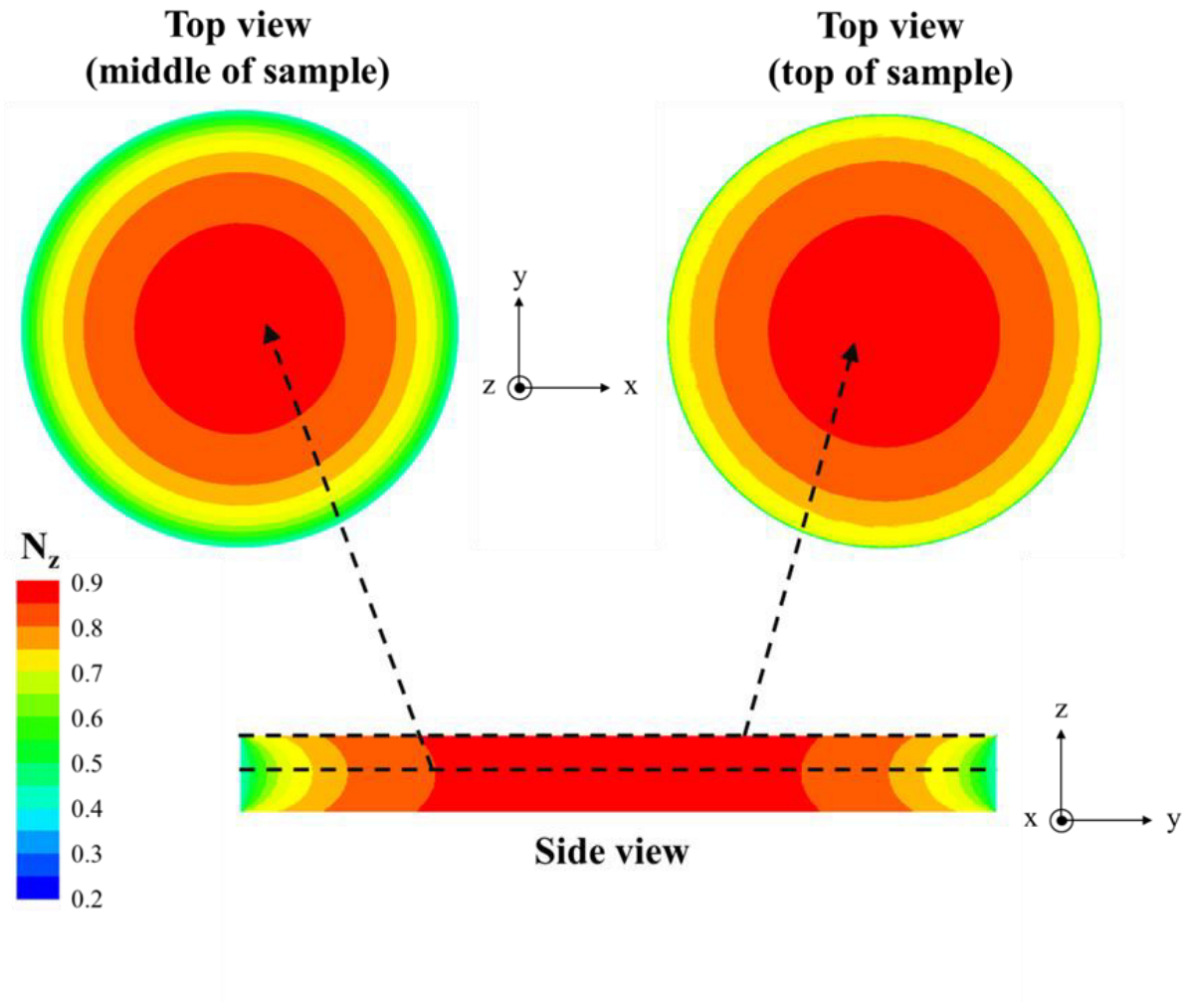

Figure 16

Spatial distribution of the N_z coefficient in a flat disk of ferrite calculated with FE simulator.

The effect of shape, and thus of the demagnetizing field, can be taken into account in the calculation of dynamic permeability by using the following equations (H_{DC} applied along z-axis):

$$\mu = 1 + \frac{\omega_m\left(\omega_0+\omega_m(N_y-N_z)\right)+j\omega\alpha\omega_m}{\left(\omega_0+\omega_m(N_x-N_z)\right)\left(\omega_0+\omega_m(N_y-N_z)\right)-\omega^2(1+\alpha^2)+2j\omega\alpha\omega_0} \quad (19\text{ a})$$

$$\kappa = \frac{\omega\omega_m}{\left(\omega_0+\omega_m(N_x-N_z)\right)\left(\omega_0+\omega_m(N_y-N_z)\right)-\omega^2(1+\alpha^2)+2j\omega\alpha\omega_0} \quad (19\text{ b})$$

As an example, permeability was calculated for different shapes of samples in the case of a ferrite (Fig. 17), with the following properties: M_s = 23873 A.m^{-1}, α = 0.1, H_{DC} = 70000 A.m^{-1}. As $N_z = N_y = N_x$ for a sphere, calculated permeability is similar to that of an infinite ferrite (without taking into account shape effect); ferromagnetic resonance frequency is thus only dependent on the internal magnetic field. This consideration explains why spherical samples are used to extract the anisotropy field of ferrites. A flat sample (flat disk) leads to a lowering of FMR due to the effect of the strong demagnetizing fields. On the contrary, long samples (a long cylinder) induce an increase of FMR due to the decrease of N_z coefficient compared with spherical samples. Moreover, the shape of the ferrite sample has an impact on the level of permeability at frequencies lower than the FMR. As an example, at 200 MHz, the permeability of a flat disk will be 1.53, and one of a long cylinder will be 1.29. The difference is greater than 18% and can lead to a frequency shift when such materials are used to fabricate antennas or filters.

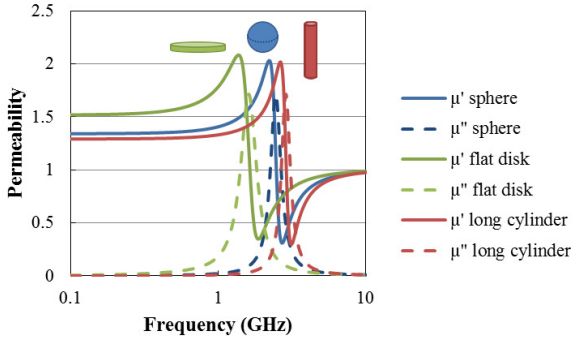

Figure 17

Calculated permeability for different shapes of ferrite (M_s = 23873 A.m^{-1}, α = 0.1, H_{DC} = 70000 A.m^{-1}).

Taking into account shape effect and demagnetizing field inhomogeneity can be crucial in the modeling of ferrite-based devices. As an example, in Thalakkatukalathil V.V.K et al 2018, a microstrip circulator in Low Temperature Co-fired Ceramics (LTCC) technology was designed and measured. This component uses a ferrite disk biased by a magnet and surrounded by a dielectric substrate. At first, the design was performed by considering a uniform internal field in the ferrite sample. Measurement showed that the bandwidth in which isolation level is lower than -15 dB was broader in measurement than in simulation (Fig. 18). Then, multiphysics simulation, that allows taking into account the non uniformity of internal static magnetic field, was performed by coupling a magnetostatic analysis of the structure and an electromagnetic computation. Such analysis provides a better agreement between simulation and measurement and demonstrates the interest to consider the spatial inhomogeneity of internal static magnetic field in the ferrite sample in the design of ferrite-based devices.

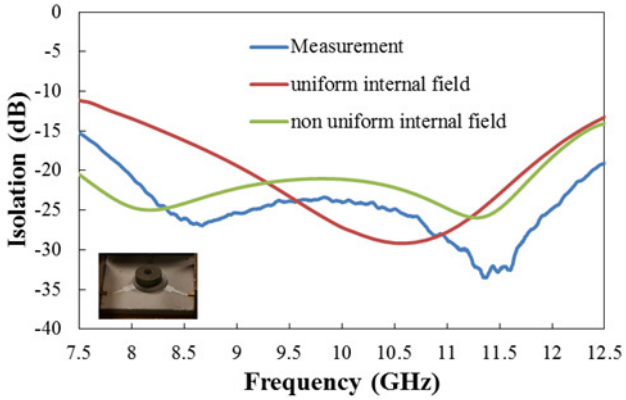

Figure 18

Isolation of a LTCC circulator in the 7.5-12.5 GHz frequency band: comparison between measurement, simulation with a uniform internal field and simulation with a non uniform internal field.

2.a.5 Dynamic demagnetizing aspect : the Polder-Smit effect

In the case of a unsaturated magnetic volume, the interactions between the magnetic domains (Fig. 1) lead to dynamic demagnetizing effects.

This situation was studied by Polder and Smit (Polder D. and Smit J. 1953). The authors establish that the AC field acting on the domains is not only constituted by the field associated with the electromagnetic wave, but also includes dynamic demagnetizing fields with depending on the orientation of the domains, as well as to the material's shape. For a better understanding of the phenomenon, we will consider a demagnetized ellipsoidal material, with lamellar magnetic domains, as depicted in Fig. 17. From domain to domain, the magnetization

points in reverse direction named “up” and “down” directions. When exposed to an AC field $\vec{h}$ the “up” and “down” magnetization will precess in opposite way. If $\vec{h}$ is perpendicular to the magnetic walls, the normal component of magnetization $\vec{m}$ is continuous, therefore no dynamic demagnetizing field exists. However, if $\vec{h}$ is parallel to the magnetic walls, then there is no continuity of the normal component of magnetization $\vec{m}$, and a dynamic demagnetizing field appears.

The intensities of the dynamic demagnetizing fields are distributed in the range $[0, M_S]$. The corresponding resonance pulsations (or frequencies) vary between $\omega_{min}=2\pi\mu_0\gamma H$ and $\omega_{max}=2\pi\mu_0\gamma(H+M_S)$. Consequently, the χ'' peak is enlarged, meaning that the absorption is generated between these two pulsations.

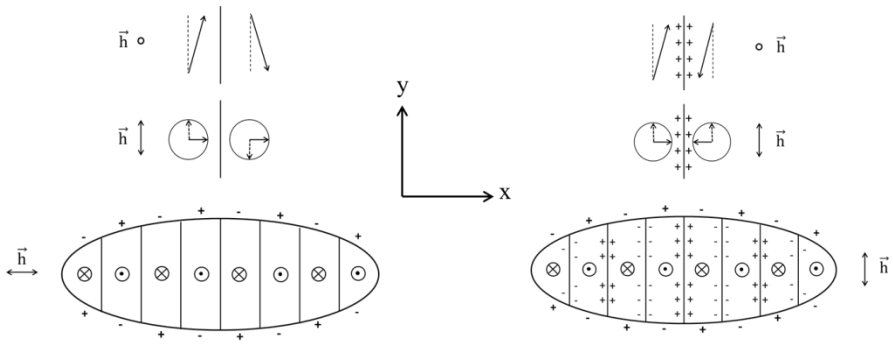

Figure 19

Depiction of the Polder-Smith effect (Adapted from Polder D. and Smit J. 1953)

2.a.6 Modeling the dynamic permeability of polycrystalline ferrites in any magnetization state

In actual materials nonuniformity of the internal field in ferrite prevents some regions from being saturated. Therfore other formulations of the permeability tensor are necessary to accurately predict the dynamic permeability of the ferrite medium. Different empirical models that provided formulas for the elements of $\bar{\bar{\mu}}$ have been proposed. Shlömann studied the case of a demagnetized body, the magnetic domains of which were randomly distributed along the three directions. Taking into account the magnetic domains magnetized along opposite directions, the off-diagonal elements of the tensor vanish. Then a mean permeability can be calculated (Schlömann E. 1970). On the basis of Schlömann’s model, and asuming a magnetic body constituted of up and down magnetic domains, Igarashi and Naito calculated the permeability tensor elements (Igarashi M. and NaitoY. 1977; Igarashi M. and NaitoY. 1981). Under the hypothesis that the magnetocrystalline field is the only contribution through the dc internal field, and also assuming that the actual frequency is far from the resonance frequency, Rado expressed the permeability tensor elements based on a spatial average of the magnetic domains (Rado, G.T. 1953). Starting from experimental results on the measurements of permeability tensor elements, Green and Sandy deduced an empirical expression of the tensor, that suits with Schlömann theory (Green J.J. and F. Sandy 1974). However the first

theoretical and predictive model that allowed the determination of the permeability tensor of polycrystalline ferrites regardless of their magnetization state was proposed by Gelin and Berthou (Gelin P. and Berthou-Pichavant K. 1997; Gelin P. et al. 2005). Thereafter Gelin and Queffelec introduced the generalized permeability tensor (GPT) model which improved accuracy in the description of the magnetic losses phenomena (Gelin P. and Queffelec P. 2008). This model remains the only predictive model for the permeability tensor of polycrystalline ferrites in any magnetization state (Guennou A et al 2007 ; Nino J. P. C. et al 2015 ; Le Gouellec A .et al.2016).

3. Microwave passive Components using ferrites

3.a Wave propagation in magnetized ferrimagnetic materials

The aim of this section is to briefly describe the basis of physical phenomena (usually termed Faraday effect) that are exploited by nonreciprocal microwave devices, such as circulators and isolators. A wave that propagates in a parallel manner to a static field H can be represented by two contra-rotating circularly polarized components. Permeabilities can then be defined for the positive and negative rotation directions. The positive direction is clockwise when viewed in the direction of H.

We consider an electromagnetic wave to be linearly polarized, with the direction of propagation directed along the static field $\vec{H}$, arbitrary assumed to go along the z-axis. The electromagnetic field $\vec{h}$ can be divided into two components with clockwise circular polarization $\vec{h}_+$ and conterclockwise circular polarization $\vec{h}_-$ around z. An effective magnetic permeability, μ^+ and μ^- respectively, is calculated for each of them (Epstein P.S. 1956). They write:

$$\mu^{\pm} = \mu \pm \kappa \tag{20}$$

where μ and κ are given by equations (5) and (6).

Their real and imaginary parts expressed as:

$$\mu^{+'}(\omega) = 1 + \frac{\omega_m(\omega_0-\omega)}{(\omega_0-\omega)^2+\alpha^2\omega^2} \tag{21a}$$

$$\mu^{+''}(\omega) = \frac{\omega_m\alpha\omega}{(\omega_0-\omega)^2+\alpha^2\omega^2} \tag{21b}$$

$$\mu^{-'}(\omega) = 1 + \frac{\omega_m(\omega_0+\omega)}{(\omega_0+\omega)^2+\alpha^2\omega^2} \tag{21c}$$

$$\mu^{-''}(\omega) = \frac{\omega_m\alpha\omega}{(\omega_0+\omega)^2+\alpha^2\omega^2} \tag{21d}$$

The plots on Fig. 18 show that $\mu^{-\prime\prime}$ is very close to zero, and that $\mu^{-\prime}$ remains almost constant. This demonstrates that the counterclockwise polarized wave weakly interacts with the magnetic material. Whereas the propagation of the clockwise polarized wave is strongly influenced by the propagating magnetic medium.

An alternative expression is often presented that gives the complex permeability as a function of the static field. Remembering that $\omega_0 = \gamma H$ and $\omega_m = \gamma$, the complex permeability μ^+ can be written as follows:

$$\mu^{+\prime}(H) = 1 + \frac{\omega_m(^{\omega_0}/_{\gamma} - H)}{(^{\omega_0}/_{\gamma} - H)^2 + \frac{\Delta H^2}{4}} \tag{22a}$$

$$\mu^{+\prime\prime}(H) = \frac{\omega_m \frac{\Delta H}{2}}{(H - ^{\omega_0}/_{\gamma})^2 + \frac{\Delta H^2}{4}} \tag{23b}$$

ΔH is the gyromagnetic line width, defined as the half width of the resonance peak $\mu^{+\prime\prime}$.

The components $\mu+\prime$ (dispersive) and $\mu+\prime\prime$ (dissipative) of the permeability tensor elements are shown on fig (20), as functions of the reduced applied field (H/H_0) and of the reduced applied frequency (ω/ω_0). The medium was assumed to be magnetically saturated.

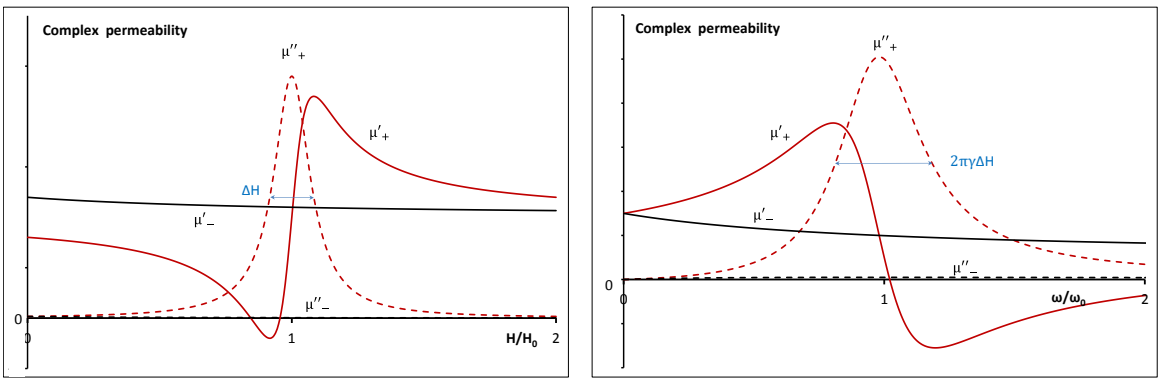

Figure 20

Plots of the real and imaginary parts of the effective magnetic permeabilities μ^+ and μ^- as a function of the reduced field (left side) and of the reduced angular frequency (right side).

The expressions for $\mu^{-\prime}$ and $\mu^{-\prime\prime}$ are as follows :

$$\mu^{-\prime}(H) = 1 + \frac{\omega_m(^{\omega_0}/_{\gamma} + H)}{(^{\omega_0}/_{\gamma} + H)^2 + \frac{\Delta H^2}{4}} \tag{24a}$$

$$\mu^{-''}(H) = \frac{\omega_m \frac{\Delta H}{2}}{(H+{}^{\omega_0}/_{\gamma})^2+\frac{\Delta H^2}{4}} \quad (24b)$$

3.b Microwave magnetic losses

In order to caracterize losses at ferromagnetic resonance, usual experiments consist in power absorption measurements : a constant high frequency AC field is applied simultaneously to a DC field of variable magnitude, that should be strong enough to ensure magnetic saturation. A plot of the absorbed power as a function of the dc field magnitude, at given frequency make it possible to obtain the resonance peak. ΔH is the peak width at half-power, it is sometime known as the absorption peak, or linewidth. It defined the magnetic losses at frequencies close to the magnetic gyroresonance appearing when the static magnetic field value allows an in-phase precession of the magnetic moments with the electromagnetic field h. Apart from the case of microwave absorbing materials, which is beyond the scope of this article, the absorption peak ΔH should be narrow. However in a polycrystaline material the actual internal field depends on many factors: magnetic anisotropy, magnetization state, porosity, eddy currents, and inhomogeneous demagnetization (Alvarez G.et al. 2010). Consequently, the broadening of ΔH is due not only to the intrinsic damping of the spins (ΔH_{int}), but it contains in addition contributions from inner demagnetizing effects (ΔH_p), linked to porosity, or more generally to a residual non magnetic part, to the influence of the magnetocrystalline anisotropy H_A. Significant contributions to linewidth also arise from inhomogeneous demagnetization field. An expression commonly used for the total linewidth ΔH was proposed by Schlöman (Schlömann E. 1958): $\Delta H = \Delta H_{int} + 1.5pM_s + H_A$ where ΔH_{int} is the intrinsic line width, p represents the volume fraction of non magnetic part. The relationship between the damping factor α and ΔH_{int} , in the case of a saturated material, is $\alpha=\gamma\frac{\Delta H}{2\omega}$ (ω beeing the angular frequency at which ΔH is measured). In a first approximation, one has $H_A = \frac{K_1}{\mu_0 M_s}$, where K_1 is the first order magnetocrystalline anisotropy constant.

However ΔH, as defined by the Polder model of precession close to the gyroresonance, is unable to describe the full range of experimental data. This is why a complementary way means to described the magnetic losses distant from the gyroresonance is needed : an effective peak can be extrapolated from the values of the permeability away from resonance. ΔH_{eff} is the effective linewidth of the half-power peak of a Lorentz curve fitting experimental values away from the resonance. ΔH_{eff} corresponds to the off-resonance magnetic losses, its values is lower than that of ΔH. This point will be illustrated in section 4b.

3.c Antenna miniaturization

Miniaturization of electronic devices for mobile communication has led to increasing demands for the reduction of antenna dimensions. Antenna downsizing is one of today's most important challenges for antenna designers (Skrivervick A.K. et al. 2001). Antenna miniaturization for wireless communication systems was first achieved through optimizing antenna design, but no other notable breakthroughs have been reported in this domain. The use of high-permittivity substrates has also allowed size reduction. The use of high-permittivity substrates also allowed size reduction, but causes a considerable decrease in antenna efficiency and bandwidth (Hwang Y. et al. 1995, Hansen R.C. 1982) . For applications in the low-UHF frequency band (300-862 MHz), the use of magneto-dielectric substrates is expected to overcome these limitations by offering larger bandwidths and improved efficiency (Hansen R.C. and Burke M. 2000, Mosallaei H.and Sarabandi K. 2004). Indeed it has been shown (Niamien C. et al. 2011, Niamien C. et al. 2014) that, although the permittivity (ε') increases the impact of losses, as well as the stored energy, the permeability (μ') plays the opposite role by decreasing them. As a consequence, the negative impact of ε' on radiation efficiency and bandwidth is counterbalanced by the positive impact of μ'. Eventhrough at frequencies lower than 30 MHz, typically, domain walls contribution to the permeability induces prohibitive losses, several solutions exist that allow this problem to be avoided : doping by Cobalt allows domain walls pinning, the use of monodomain particles may also make it possible to limit losses.

Spinel ferrites, which have ε'>1 and μ'>1, together with low loss tangents (both dielectric and magnetic), are among the best candidates for antenna downsizing (Mattei J.-L et al. 2011, Huitema L. et al. 2013, Kong L.B et al.2013, Petrov R et al. 2008, Kabalan A. et al. 2019).
Fig. 21 shows antenna's length reduction allowed by the use of a magnetodielectric ferrite (the ferrite is in blue color). In this exemple the operating antenna frequency is 130 MHz. In order to preserve a light weight to the device, the ferrite material was placed only where the electrical currents were large (Kabalan A. et al. 2019.) Various antennas topologies were studied, the more important antenna miniaturization reached 61% (Fig. 21 c).

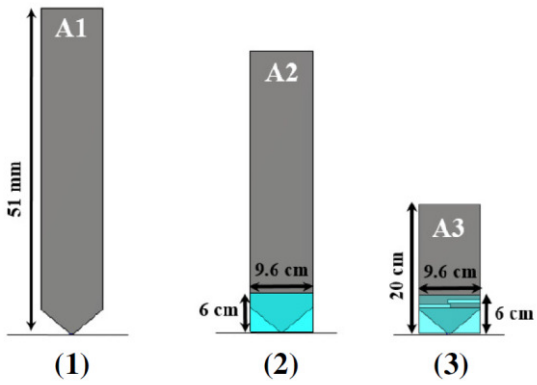

Figure 21

Exemple of antenna's length reduction allowed by the use of a magnetodielectric ferrite (the ferrite is in blue color). The operating antenna frequency is 130 MHz. Various antennas

topologies were studied, the more important antenna miniaturization reached 61% (Kabalan A. et al. 2019.)

3.d Isolators and circulators

Non-reciprocal devices, such as circulators and isolators are among the most important applications of self-biased hexaferrites in the microwave frequency range. These devices make it possible to isolate the incoming signal from the outgoing signal in transmitter/receiver (Tx/Rx) modules (Fig. 22).

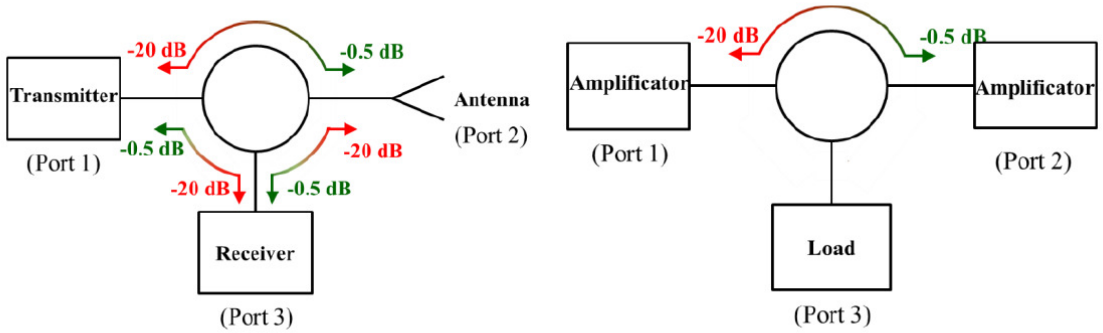

Figure 22

Schematic representation of signal transmission through a circulator (left-hand diagram) and an isolator (right-hand diagram). For devices such these ones, the propagation of electromagnetic waves is different in direct (port 1 to port 2) and reverse (port 2 to port 1) directions of propagation (adapted from Harris V.G. and Sokolov A.S. 2019).

The magnetic polarization of non-reciprocal devices can be achieved through permanent magnets, placed on both sides of the ferrite (Fig. 23). However, because doing this goes against the miniaturization and lightness objectives of modern communication applications, it is highly desirable to use self-polarized hard ferrites with reduced remanent magnetization value near to $M_R/M_S = 0.85$ (Fig.24). The device operates then at the remanent state of the ferrite. In this field, hard ferrites show great potential for integration into non-reciprocal microwave devices at frequencies from 10 to 40 GHz (Pullar R.C.2012, Sakai T. et al. 2006, Harris V.G. et al. 2009).

Microwave systems that use a single antenna for signals emission and reception need in turn to use a circulator. For device such as a circulator, the propagation of electromagnetic waves is different in direct (port 1 to port 2) and reverse (port 2 to port 1) directions of propagation (Fig. 22). This is particularly true in the case of self-biased ferrites (which are magnets that remain in a magnetized state in the absence of an externally applied magnetic field).

Isolators are another example of nonreciprocal microwave devices. They are used when it is necessary to isolate the device of a high-power amplifier (Fig. 22).

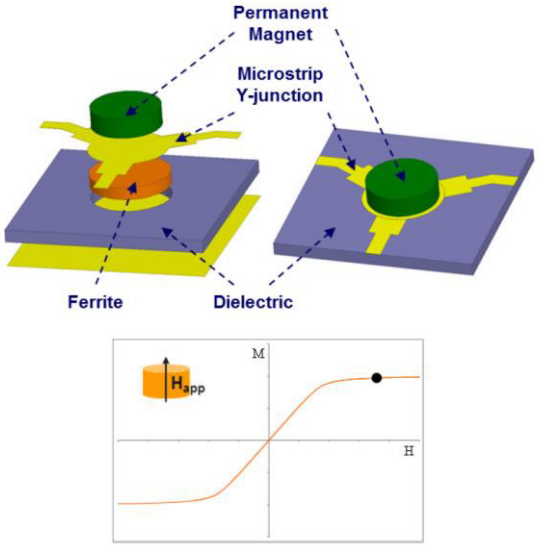

Figure 23

Drawning of a Y-junction circulator (exploded view in the figure to the left). The ferrite puck is magnetized at saturation by the prominent bias permanent magnet.

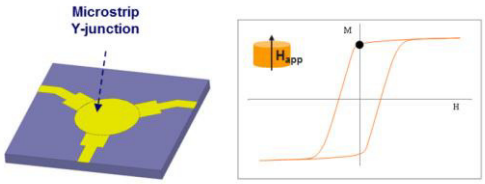

Figure 24

Drawning of a seld-biased Y-junction circulator. The self polarized hexaferrite puck (BaM type), placed below the microstrip-Y junction, is used at the remanence.

4 Microwave characterization methods:

In this section, we summarize some characterization methods of material properties at microwave frequency. An exhaustive review of characterization methods can be found in Chen L. F 2004. The electromagnetic parameters of interest for microwave applications are the complex permittivity, the initial complex permeability for demagnetized materials, the complex permeability tensor and the ferromagnetic linewidth for magnetized materials. Measurement methods for these parameters generally fall into two categories: (i) resonant

methods, which allow high accuracy but narrowband measurements and (ii) non-resonant methods, which allow broadband measurements but low accuracy. All of them use network analyzers to measure S parameters of a measurement cell, which takes form of a resonant cavity in the first case and transmission line or waveguide in second case.

4.a Characterization of demagnetized samples

If the ferrite is demagnetized, then the sample shows isotropic properties and its permittivity and permeability are complex scalar quantities that can be determined from the measurements of two measured complex S parameters: the reflection coefficient S11 and transmission coefficient S21(Baker-Jarvis J. 2005). A coaxial transmission line and rectangular waveguide (Fig. 25) are the broadband characterization methods most frequently used because analytical relationships exist between the S parameters, dimensions of the measurement cell and electromagnetic parameters when samples completely fill the cross section of the cell (Weir W. B. 1974, Nicolson A. and Ross G. 1970).

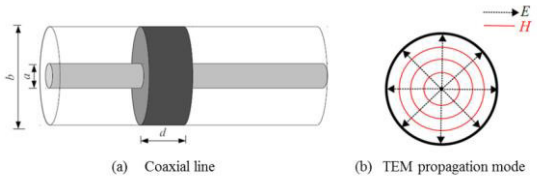

(a) Coaxial line (b) TEM propagation mode

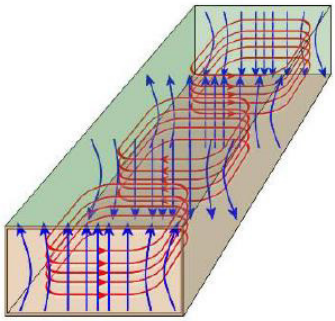

(c) rectangular waveguide

Figure 25

Sketch and electromagnetic field pattern of coaxial transmission line (a, b) and rectangular waveguide (c)

The coaxial transmission line method offers many advantage over the rectangular waveguide method. First, the frequency band is broader because there is no lower cut-off frequency in

coaxial line for the TEM (transverse electromagnetic) mode and second the sample's shape is well adapted to the magnetic field pattern avoiding demagnetizing effects. Usual measurement frequency band in coaxial method starts from 1 MHz (depending on the VNA sensibility) up to 18 GHz (the frequency of occurrence of the first higher order mode in APC7 standard).

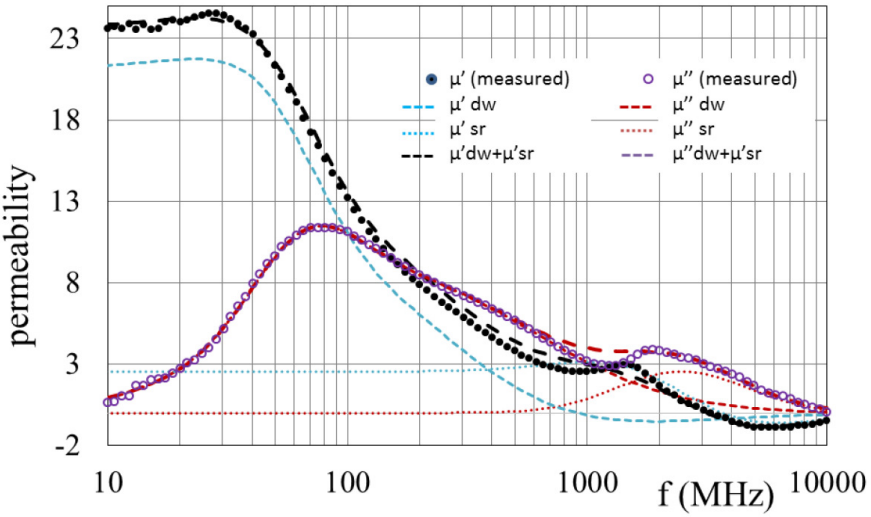

Figure 26

Measured permeability of NiFeO material from coaxial transmission line method, and its fit by spin rotation and domain wall contributions. The labels dw and sr are for domain wall and spin rotation, respectively. Spin rotation and domain wall movements contributions to the magnetization are distinguished. The total permeability is the sum of these two contributions.

Figure 26 shows the measured permittivity and permeability for a polycrystalline demagnetized nickel ferrite. The imaginary part of the initial permeability shows two maxima: the first, around 80 MHz, is associated with the domain wall motion and the second, close to 1800 MHz, is the gyromagnetic resonance related to the anisotropy field H_k ($Fr = \gamma H_k$). The permittivity of ferrite is generally not dispersive and remains constant over the whole frequency band, with values ranging from 10 to 20 but generally remaining close to 15.

4.b Characterization of magnetized samples

If the ferrite is magnetized, the sample shows anisotropic properties and the permeability becomes a complex tensor quantity with extra-diagonal terms (the permittivity does not depend on the magnetic state of the sample and remains a scalar quantity). The non-diagonal permeability tensor is the most important property used in microwave devices to reach non-reciprocal behavior.

For saturated ferrites, the permeability is well described by the Polder's model. The gyromagnetic resonance linewidth ΔH is then the fundamental property used to describe the dynamic magnetic losses. Resonance linewidth ΔH is defined as the difference between the applied field values at which absorption is half of the maximum value. Standard method for measuring the resonance linewidth ΔH of ferrites is by using resonant cavities as described in IEC standard (IEC 1982). This method is based on the cavity perturbation theory, which requires a sample's dimensions to be smallerthan one quarter of the wavelength of the microwave radiation in the sample. This method is limited to a single frequency that corresponds to the resonant frequency of the measurement cavity (generally operating around 9.4 GHz).

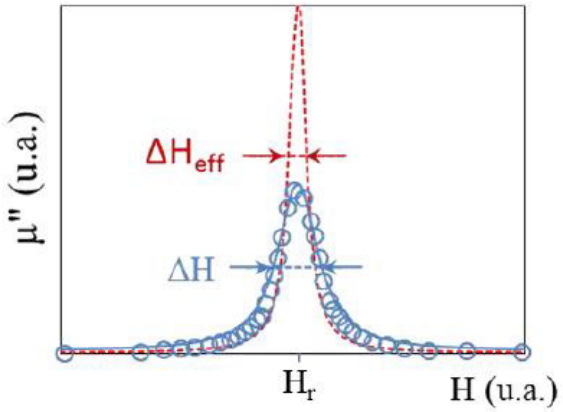

Figure 27

Measured magnetic losses from a cavity method at 9.4GHz. ΔH is the linewidth of the Lorentzian curve near the resonance (Hdc≈ Hr). ΔH_{eff} is the linewidth of the Lorentzian curve outside the vicinity of the resonance (Hdc ≠ Hr).

Figure 27 shows the absorption of the ferrite as a function of the applied magnetic field. ΔH is the linewidth of the Lorentzian curve along the experimental points near the resonance (Hdc≈ Hr). ΔH_{eff} is the linewidth of the Lorentzian curve along the experimental points outside the vicinity of the resonance (Hdc ≠ Hr).

For partially magnetized ferrites, various characterization techniques have been developed to characterize the anisotropic properties of the materials. In the resonant method, the aim is to identify and control the direction of the microwave magnetic field in the cavity so that the corresponding component of the permeability tensor can be measured. Most resonant methods use cylindrical or rectangular degenerate mode cavities or a ring resonator (Ogasawara N. 1976, Krupka J. et al. 1996). These resonant methods only work at a single or several discrete

frequencies and are very suitable for low-loss materials but not pertinent at the resonance frequency where the values of losses are high.

In reflection/transmission methods, it is essential to measure more than two S parameters in order to determine the three unknowns electromagnetic parameters ε, μ and the extra-diagonal term κ. To do this, measurement cells are asymmetrically filled to present nonreciprocal behavior taking advantage of the field displacement effect in the magnetized magnetic material.

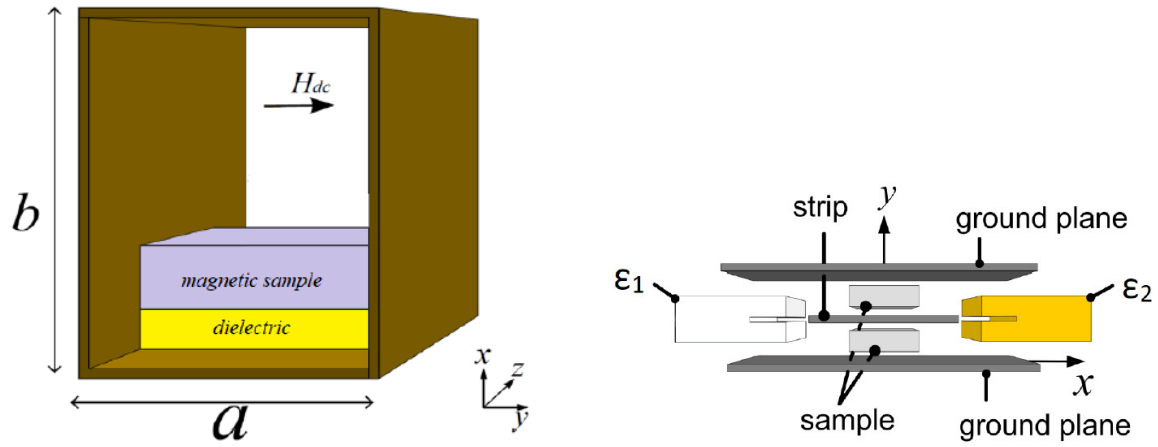

Figure 28

Diagram of asymmetrical cells : rectangular waveguide and strip transmission line

Figure 28 shows schemes of two methods based on (i) an asymmetrically loaded rectangular waveguide (Queffelec P. et al. 2000) and (ii) an asymmetrically loaded strip line (Lezaca J. E et al. 2010 , Lezaca J. E et al. 2011). In the latter method, the measurement cell consists of an asymmetric strip line partially filled with the material to be characterized. Two identical magnetic samples are placed above and below the metal strip. Two dielectrics with different permittivity values (ε_1, ε_2) are placed on each side of the strip line to ensure the nonreciprocal behavior of the structure ($S12 \neq S21$) when the magnetic sample is magnetized. In the forward direction of EM wave propagation, there is a strong wave-material interaction with dielectric 1. In the backward direction, thanks to the field displacement effect, the EM wave interacts with dielectric 2. This nonreciprocal nature of the measurement cell makes it possible to determine the diagonal component μ and extra-diagonal component κ of the permeability tensor. This method is based on a full-wave analysis, taking into account higher order modes (propagated in the loaded section and evanescent in the air sections of the measurement cell).

By associating specific broadband optimization it is possible to find the electromagnetic parameters of the unknown material while minimizing the difference between experimental and theoretical S-parameters. Experimental results (Chevalier A. et al 2013) of the permeability tensor component μ and κ of a garnet ferrite are shown in Figure 29.

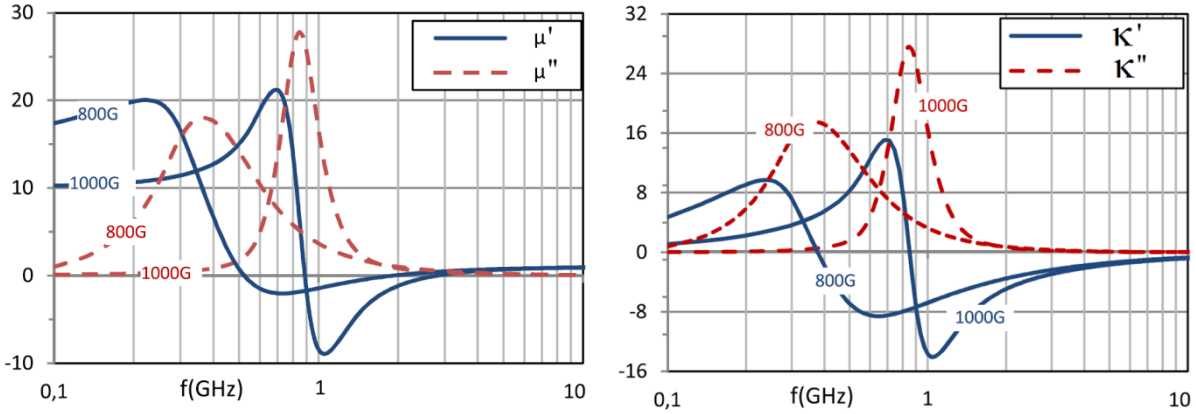

Figure 29

Measured permeability tensor components for a garnet ferrite under applied static magnetic field up to 1000 Oe.

Bibiography

Aharoni A. 1998 *Demagnetizing factors for rectangular ferromagnetic prisms*, J. Appl.Phys. **83** 3432-34

Alvarez G., Montiel H., Barron J.F., Gutierrez M.P., Zamorano R. 2010 *Yafet–Kittel-type magnetic ordering in $Ni_{0.35}Zn_{0.65}Fe_2O_4$ ferrite detected by magnetosensitive microwave absorption measurements* Journal of Magnetism and Magnetic Materials **322** 348–352

Baker-Jarvis J. 2005 *Measuring the permittivity and permeability of lossy materials: Solids, liquids, metals, building materials, and negative-index materials* NIST Tech. note 1536, 2005.

Chen Du-Xing, Brug J. A. and Goldfarb R. B. 1991, *Demagnetizing factors for cylinders* IEEE Trans. Magn. **27**, 3601-19

Chen L. F., Ong C., Neo C. P., Varadan V., and Varadan V. K 2004. *Microwave electronics: measurement and materials characterization*, Wiley & So.

Chevalier A., Cortes J., Lezaca J., and Queffelec P. 2013 *Broadband permeability measurement method for ferrites at any magnetization state: Experimental results* J. Appl. Phys **114(17)** 174904

Epstein P.S. 1956 *Theory of Wave Propagation in a Gyromagnetic Medium* Reviews of Modern Physics **28(1)** 3-17

Gelin P. and Berthou-Pichavant K. 1997 *New consistent model for ferrite permeability tensor with arbitrary magnetization state* IEEE Trans. Microw. Theory Techn. **45**(8) 1185–1192

Gelin P., Queffelec P. and Le Pennec F. 2005 *Effect of domain shapes on the dynamical behavior of polycrystalline ferrites: Application to the initial permeability* J. Appl. Phys. **98**(5)

Gelin P. and Queffelec P. 2008 *Generalized permeability tensor model: Application to barium hexaferrite in a remanent state or self-biased circulators*. IEEE Trans. Magn. 44(1) 24–31

Gilbert T. L. 1955 *A Lagrangian formulation of the gyromagnetic equation of the magnetization field* Phys. Rev **100** no. 4 1243-1255

Green J.J. and F. Sandy 1974 *Microwave characterization of partially magnetized ferrites.* IEEE Transactions on Microwave Theory and Techniques **22**(6) 641-645

Guennou A., Della B., Quéffélec P., Gelin P., and Mattei J. L. 2007. *Influence of the Magnetic Field Nonuniformity on an X-Band Microstrip Y-Junction Circulator Bandwidth: Theory/Experiment Comparison*. IEEE Transactions on Magnetics **43**(6) 1642-44

Goldman A. 2006 *Modern ferrite technology*. 2_{nd} Ed, Springer ed.

Hansen R.C. 1982 *Fundamental limitations in antennas*. Proceedings of the IEEE **69(2)**, 170-82

Hansen R.C. and Burke M. 2000 *Antennas with magneto-dielectrics* Microw. Opt. Techno. Lett. **26** 75–8

Helszajn J. 2008, *The Stripline Circulator: Theory and Practice*, Ed. John Wiley and Sons

Harris V.G., Chen Y., ChenZ., and Geiler A.L. (2014) *Tuning of Structure and Magnetic Anisotropy in Microwave Ferrites* J. Jpn. Soc. Powder Powder Metallurgy **61** Supplement S1 S273

Harris V.G., Geiler A., Chen Y., Yoon S.D., Wu M., Yang A., Chen Z., He P., Parimi P.V., Zuo X., Patton C.E., Abe M., Acher O., Vittoria C. 2009 *Recent advances in processing and applications of microwave ferrites* J. Magn. Magn. Mater. **321**.

Harris V.G. and Sokolov A.S. 2019 *The self-biased circulator: ferrite materials design and process considerations.* Journal of Superconductivity and Novel Magnetism **32** 97–108

Hwang Y., Zhang Y.P., Zheng G.X., Lo T.K.C.1995, *Planar inverted F antenna loaded with high permittivity materia.* Electron. Lett. **31** 1710–12.

Igarashi M. and NaitoY. 1977 *Tensor permeability of partially magnetized ferrites.* IEEE Transactions on Magnetics **13**(5) 1664-1668

Igarashi M. and NaitoY. 1981 *Parallel Component μ z of Partially Magnetized Microwave Ferrites.* IEEE Transactions on Microwave Theory and Techniques **29**(6) 568-571

IEC 1982 *Measuring methods for properties of gyromagnetic materials intended for application at microwave frequencies* **IEC 60556**, 1982.

Huitema L., Reveyrand *T.*, Mattei J.L., Arnaud E., Decroze C, Monedière T. 2013 *Frequency Tunable Antenna Using a Magneto-Dielectric Material for DVB-H Application* IEEE Trans. Ant. Propag. **61(9)** 4456-66

Joseph R.I.and Schlöemann E. 1965 *Demagnetizing Field in Nonellipsoidal Bodies*.J. App. Phys.**36** no. 5 1579-93

Kabalan A., Sharaiha A., Tarot A-C. 2019 *Enhance the impact of the magneto-dielectric materials to miniaturize a planar monopole antenna* 2019 URSI Asia-Pacific Radio Science Conference (AP-RASC) 9-15 March 2019, DOI: 10.23919/URSIAP-RASC.2019.8738556 see also Kabalan A., Sharaiha A., Tarot A-C *Optimization of the use of magneto-dielectric materials for highly miniaturized monopole antennas 2019* 13th European Conference on Antennas and Propagation (EuCAP) 31 March-5 April 2019

Kong L.B., Li Z.W., Liu L., Huang R., Abshinova M., Yang Z.H 2013. *Recent progress in some composite materials and structures for specific electromagnetic applications*. Int. Mater. Rev. **58** 203–259.

Krupka J. and Geyer R. G. 1996 *Complex permeability of demagnetized microwave ferrites near and above gyromagnetic resonance*. IEEE Trans. Magn. **32(3)** 1924–33

Landau L and Lifshitz E. 1935 *On the theory of the dispersion of magnetic permeability in ferromagnetic bodies*. Phys. Z Sowjetunion **8** 153-169; Landau L. Collected Papers, edited by D. ter Haar (Gordon and Breach, New York), p. 101, 1965. L. D. Landau and E. M. Lifshitz, Electrodynamics of Continuous Media.Oxford, U.K.: Pergamon Press, 1984

Le Gouellec A., Verissimo G., Laur V., Queffelec P., Albert I., and Girard T. 2016 *Modeling non-saturated ferrite-based devices: Application to twin toroid ferrite phase shifters*. J. Appl. Phys. **120(7)** 073902

Lezaca J. E., Queffelec P., and Chevalier A. 2010 *Generalized Measurement Method for the Determination of the Dynamic Behavior of Magnetic Materials in Any Magnetization State* IEEE Trans. Magn **46(6)** 1687–90.

Lezaca J. E., Queffelec P., and Chevalier A. 2011 *Broadband permeability measurement method for ferrites at any magnetization state: direct problem* Int. J. Microw. Wirel. Technol. **3(3)** 289–94

Mattei J.-L., Huitema L., Queffelec P., Pintos J.-F., Minard P., Sharahia A. 2011 *Suitability of Ni-Zn Ferrites Ceramics With Controlled Porosity as Granular Substrates for Mobile Handset Miniaturized Antennas.* IEEE Trans. Magn. **47** 3720–23.

Mattei J-L., E. Le Guen, Chevalier A., Tarot A.C. 2015 *Experimental determination of magnetocrystalline anisotropy constants and saturation magnetostriction constants of Ni-Zn and Ni-Zn-Co ferrites intended to be used for antennas miniaturization* Journal of Magnetism and Magnetic Materials **374** 762–68

Mikami I.1973 *Role of induced anisotropy in magnetic spectraof cobalt-substituted nickel-zinc ferrites*. Japanese Journal ofApplied Physics **12** no.5 678–693

Mosallaei H.and Sarabandi K. 2004 *Magneto-dielectrics in electromagnetics: Concept and applications*, IEEE Trans. Antennas Propag. **52** 1558–67.

Niamien C., Collardey S., Sharaiha A., Mahdjoubi K. 2011 *Compact Expressions for Efficiency and Bandwidth of Patch Antennas Over Lossy Magneto-Dielectric Materials* IEEE Antennas Wirel. Propag. Lett. **10** 63–66

Niamien C., Collardey S., Sharaiha A., Mahdjoubi K. 2014 *Printed inverted-F antennas over lossy magneto-dielectric materials: Theoretical approach and validations* IET Microwaves, Antennas Propag**. 8(7)** 513–22

Nicolson A. and Ross G. 1970 *Measurement of the intrinsic properties of materials by time-domain techniques* IEEE Trans. Instrum. Meas. **IM-19(4)** 377–82.

Nino J. P. C., Queffelec P., and Chevalier A. 2015 *Modeling antennas printed on magnetized substrate: Application to the design of a tunable PIFA antenna*, in Proc. 45th European Microwave Conf. 933–936

Ogasawara N., Fuse T., Inui T., and Saito I. 1976 *Highly sensitive procedures for measuring permeabilities ($\mu\pm$) for circularly polarized fields in microwave ferrites* IEEE Trans. Magn. **12(3)** 256–59

OPERA3D, Vector Fields, 24 Bankside, Kindlington, Oxford, UK.

Osborn J. A 1945 *Demagnetizing Factors of the General Ellipsoid* Phys. Rev. **67**, 351-57

Perekalina T.M., Askochinskii A.A., Sannikov D.G. 1961 *Resonance of domain walls in cobalt ferrite.* Soviet Physics JETP **13(2)** 303-7

Petrov R. V., Tatarenko A. S., Srinivasan G. Mantese J. V. 2008 *Antenna miniaturization with ferrite-ferroelectric composites.* Microw. Opt. Technol. Lett. **50(12)** 3154–57

Pfeiffer H. 1990 *Determination of anisotropy field distribution in particle assemblies taking into account thermal fluctuations*. *Phys. stat. sol. (a)* **118,** 295-306

Polder D. 1949 *On the theory of ferromagnetic resonance*, *Philosophical magazine* **40**, 99-115

Polder D. and Smit J. 1953 *Resonance Phenomena in ferrites*. Rev. Mod. Phys. **25**(1), 89-90

Pullar R.C.2012 *Hexagonal ferrites: a review of the synthesis, properties and applications of hexaferrite ceramics* Prog. Mater. Sci. **57** 1191–1334

Queffelec P., Le Floc'h M., and Gelin P. 2000 *New method for determining the permeability tensor of magnetized ferrites in a wide frequency range* IEEE Trans. Microw. Theory Tech. **48(8)** 1344–51.

Rado G. 1953. *Magnetic Spectra of Ferrites* Rev. Mod. Phys. **25** 81

Sakai T., Chen Y., Chinnasamy C.N., Vittoria C., Harris V.G. 2006 *Textured Sc-doped barium-ferrite compacts for microwave applications below 20 GHz.* IEEE Trans. Magn. **42** 3353–55

Schlomann E. 1958, *Ferromagnetic resonance in polycrystalline ferrites with large anisotropy* J. Phys. Chem. Solids **6(2-3)** , 257-66

Schlomann E. 1970 *Microwave behavior of partially magnetized ferrites.* Journal of applied physics **41**(1) 204-214

Skrivervik A.K., Zurcher J.F., Staub O., Mosig J.R. 2001 *PCS antenna design: The challenge of miniaturization.* IEEE Antennas Propag. Mag. **43** 12–27.

Smit, J. and Wijn, H.P.J. (1959) *Ferrites.* Philips Technical Library, Eindhoven.

Srivastava C.M. and Patni M.J. 1974 *Ferromagnetic Relaxation Processes in Polycrystalline Magnetic Insulator* Journal of Magnetic Resonance **15** 359-66

Thalakkatukalathil V.V.K., Chevalier A., Laur V., Verissimo G., Queffelec P., Qassym L., Lebourgeois R. 2018 *Electromagnetic modeling of anisotropic ferrites - Application to microstrip Y-junction circulator design* J. App. Phys. **123** 234503

Valenzuela R. 1994 *Magnetic ceramics* Cambrige University Press

Van Uitert L. G. 1955 DC Resistivity in the Nickel and Nickel Zinc Ferrite System. *J. Chem. Phys.* **23**, 1883

Wangsness R. K. 1954 *Magnetic Resonance in Ferrimagnetics*. Phys. Rev. **93**, 68

Weir W. B. 1974 *Automatic Measurement of Complex Dielectric Constant and Permeability* Proc. IEEE, **62(1)** 33-36